

Ultraviolet variability in Radio-Loud Active Galactic Nuclei observed by UVIT onboard *AstroSat*

M. Reshma^a, C. S. Stalin^b, Amit Kumar Mandal^c, S. B. Gudennavar^{1a}, Seniorita Benedict^d, Prajwel Joseph^b

^aDepartment of Physics and Electronics, CHRIST University, Bengaluru 560029, Karnataka, India

^bIndian Institute of Astrophysics, Block II, Koramangala, Bengaluru 560034, Karnataka, India

^cCenter for Theoretical Physics of the Polish Academy of Sciences, Al. Lotniko'w 32/46, 02-668 Warsaw, Poland

^dSt. Joseph's University, 36, Lal Bagh Main Road, Langford Gardens, Bengaluru 560 027, India

Abstract

Radio-loud active galactic nuclei (AGN) are among the most luminous objects in the Universe, emitting radiation from low-energy radio waves to high energy γ -rays. They are well known to exhibit flux variations at nearly all accessible wavelengths. However, their variability properties in the ultraviolet (UV) band remain relatively less explored compared to other wavebands. Here, we present the results of a systematic investigation of the UV flux and spectral variability characteristics of 24 radio-loud AGN spanning the redshift range $0.018 \leq z \leq 2.218$. The sample comprises 17 BL Lac objects, 6 flat spectrum radio quasars (FSRQs) and one radio-loud narrow line Seyfert 1 galaxy. We used observations obtained with the Ultra-Violet Imaging Telescope (UVIT) onboard *AstroSat* during its first ten years of operation, covering both the far-UV (FUV; 1300–1800 Å) and near-UV (NUV; 2000–3000 Å) bands. Of the 24 sources analysed, 18 showed significant UV variability on hour timescales. We found a bluer when brighter (BWB) spectral trend in two sources: the FSRQ CTA 102 and the BL Lac PKS 0447–439. The observed UV variability in our sample of radio-loud AGN, together with the BWB trend detected in these two sources, supports a scenario in which the hour timescale UV variations are driven by intrinsic processes within their relativistic jets.

Keywords: Active galactic nuclei, Blazars, BL Lacertae objects, Flat spectrum radio quasars, Narrow-Line Seyfert 1 galaxy, Ultraviolet variability

1. Introduction

Active galactic nuclei (AGN) are among the most luminous sources in the Universe, with luminosities in the range $10^{11} - 10^{14} L_{\odot}$. Such extreme emission is powered by the accretion of matter onto supermassive black holes (SMBHs) located at the centres of galaxies, with masses spanning 10^6 to $10^{10} M_{\odot}$ (Lynden-Bell, 1969; Rees, 1984). The accretion process that powers AGN produces radiation across the entire electromagnetic spectrum from low-energy radio waves to high-energy γ -rays. AGN are broadly classified into two main categories based on their radio properties: radio-loud AGN, which emit predominantly non-thermal radiation through powerful relativistic jets, and radio-quiet AGN, which lack prominent radio jets and whose emission is dominated by thermal radiation from their accretion disks. The fundamental distinction between these two classes lies in the presence or absence of strong relativistic jets. Approximately 15% of AGN are radio-loud (Kellermann et al., 1989). This population includes radio galaxies, blazars, and radio-loud narrow-line Seyfert 1 galaxies. However, it has been suggested that AGN need to be classified based on a physical difference into non-jetted (absence of relativistic jets; eg. Seyferts) and jetted (presence of relativistic jets; eg. blazars) AGN (Padovani et al., 2017).

Blazars constitute a prominent subclass of radio-loud AGN, and are characterized by relativistic jets oriented closely to

the observer's line of sight, typically within a viewing angle $\leq 10^{\circ}$ (Urry and Padovani, 1995). These sources exhibit rapid and large amplitude flux variability on timescales ranging from minutes to hours (Wagner and Witzel, 1995; Ulrich et al., 1997; Raiteri, 2025), spanning the entire electromagnetic spectrum from radio to γ -rays. In the high energy γ -ray band, flux variations on minute timescales have been detected in a handful of blazars (Aharonian et al., 2007a; Albert et al., 2007; Arlen et al., 2013; Ackermann et al., 2016; Shukla et al., 2018; Shukla and Mannheim, 2020; Pandey and Stalin, 2022). Blazars are further classified into two subclasses: flat spectrum radio quasars (FSRQs), which show broad emission lines with equivalent widths $> 5 \text{ \AA}$, and BL Lacertae objects (BL Lacs), which show absent or weak emission lines with equivalent widths $< 5 \text{ \AA}$ (Urry and Padovani, 1995). However, according to Ghisellini et al. (2011), the fundamental physical distinction between FSRQs and BL Lacs is based on the broad-line region (BLR) luminosity relative to the Eddington luminosity, where FSRQs are characterized by a luminous BLR satisfying $L_{\text{BLR}}/L_{\text{Edd}} > 5 \times 10^{-4}$. Their broadband spectral energy distribution (SED) typically displays a characteristic double-peaked structure. The low-energy peak, extending from the infrared to the ultraviolet (UV)/soft X-ray band, is attributed to synchrotron emission from relativistic electrons in the jet. The high-energy peak, occurring at the hard X-ray/ γ -ray region, is commonly interpreted as arising from inverse

Compton scattering of synchrotron photons (synchrotron self-Compton) or external photons (external Compton). Based on the frequency of the synchrotron peak, blazars are further categorized as low-synchrotron-peaked (LSP; $\nu_{peak} < 10^{14}$ Hz), intermediate-synchrotron-peaked (ISP; $10^{14} < \nu_{peak} < 10^{15}$ Hz) and high-synchrotron-peaked (HSP; $\nu_{peak} > 10^{15}$ Hz) sources (Abdo et al., 2010a).

Another important class of AGN is the narrow-line Seyfert 1 (NLSy1) galaxies, first identified by Osterbrock and Pogge (1985). These sources are characterised by narrow $H\beta$ emission lines with full width at half maximum $< 2000 \text{ km s}^{-1}$, $[OIII]/H\beta < 3$, prominent FeII emission, steep soft X-ray spectra, and rapid X-ray variability (Boller et al., 1996; Leighly, 1999a,b). NLSy1 galaxies are thought to host relatively low-mass black holes ($10^6 - 10^8 M_{\odot}$; Peterson et al. 2000; Grupe and Mathur 2004). Approximately 5–7% of NLSy1 galaxies are radio-loud (Komossa et al., 2006; Yuan et al., 2008; Rakshit et al., 2017). Unlike blazars, which are typically hosted by elliptical galaxies, radio-loud NLSy1 galaxies are believed to reside in spiral galaxies (Belloni, 2010), with some exhibiting large scale relativistic jets (Rakshit et al., 2018; Vietri et al., 2022; Umayal et al., 2025). A small fraction of radio-loud NLSy1 galaxies are detected as high energy γ -ray emitters by the Fermi-Large Area Telescope (Abdo et al., 2009b; Paliya et al., 2018) pointing to the presence of relativistic jets in them (D’Ammando, 2019; Foschini, 2020). They exhibit intra-night optical variability comparable to that observed in blazars (Paliya et al., 2013). Rapid variability in X-rays, UV and optical bands are also known in these objects (D’Ammando, 2020a,b). These findings suggest that the jet contributes to the observed optical and UV emission, while in X-rays, the emission likely arises from both the jet and corona. There is also a report of an NLSy1 galaxy exhibiting rapid X-ray variability, with a halving timescale of less than 30 seconds (Feigelson et al., 1986).

Variability is a defining observational property of AGN (Wagner and Witzel, 1995; Ulrich et al., 1997; Raiteri, 2025) and serves as a powerful diagnostic for probing the physical processes governing accretion and jet emission. The dominant emission mechanism in the UV band depends on both the source type and its activity state. In radio-quiet (non-jetted) AGN, the UV emission primarily arises from thermal radiation emitted by the accretion disk, typically manifested as the “big blue bump” in their broadband SED. In contrast, in radio-loud (jetted) AGN, the UV emission is largely dominated by synchrotron radiation originating from their relativistic jets. In the broadband SEDs of blazars, the UV emission is predominantly produced by synchrotron radiation from relativistic electrons in the jet (Abdo et al., 2011; Paliya et al., 2015). However, in FSRQs, during low-flux states, signatures of accretion disk emission are seen in their broadband SEDs (Paliya et al., 2016, 2017). Despite its importance, systematic studies of AGN variability in the UV regime remain relatively scarce (Paltani and Courvoisier, 1994; Welsh et al., 2011; Sukanya et al., 2018; Reshma et al., 2024). Using observations from the International Ultraviolet Explorer (IUE), Paltani and Courvoisier (1994) reported increasing variability amplitude toward shorter wave-

lengths for a large sample of AGN, while Edelson et al. (1991) detected rapid UV variability on timescales shorter than a day in the blazar PKS 2155–304. UV variability nature of AGN is therefore less understood.

In this work, we investigated the UV flux and spectral variability on hour timescales for a sample of 24 AGN, comprising one radio-loud NLSy1 galaxy, 17 BL Lacs, and 6 FSRQs using observations obtained with the Ultra-Violet Imaging Telescope (UVIT; Tandon et al. 2020) onboard *AstroSat*. Our sample selection was guided by two criteria: (a) the source must be radio-loud, and (b) the observational data must be publicly available beyond the proprietary period. Applying these criteria yielded a sample of 24 AGN. All are blazars, with the exception of 1H 0323+342, which is a radio-loud NLSy1 galaxy. However, 1H 0323+342 shares several properties with flat-spectrum quasars: it has been detected in the γ -ray band (Abdo et al., 2009b), and its broadband SED closely resembles that of FSRQs. For these reasons, we have included it in our sample. The structure of the paper is as follows: Section 2 describes the data collection and data reduction procedures. Section 3 outlines the methods employed for flux and spectral variability analysis. Notes on individual sources are given in Section 4. Results and discussion are given in Section 5, followed by the summary in the final Section 6.

2. Observations and data reduction

We utilized publicly available archival observations of radio-loud (jetted) AGN obtained with UVIT onboard *AstroSat* (Agrawal, 2017), during the first ten years of its operation following its launch by the Indian Space Research Organization, Bengaluru on 28 September 2015. UVIT has a circular field of view of approximately $28'$ in diameter and provides simultaneous imaging in the far-UV (FUV; 1300–1800 Å) and near-UV (NUV; 2000–3000 Å) bands. It also includes a visible channel (VIS; 3200–5500 Å), which is primarily used for tracking the telescope aspect. Table 1 lists the sources analysed in this work, while Table 2 provides the corresponding observation log.

We used the Level 1 data obtained from the Indian Space Science Data Center (ISSDC) to generate the science ready images. These images were generated by the UVIT Payload Operation Center (POC) at the Indian Institute of Astrophysics, Bengaluru, using version 7.0 of the UVIT Level 2 data processing pipeline (Joseph et al., 2025). The science ready images made available to ISSDC for archival and dissemination by the POC were created from the raw Level 1 data after applying corrections for spacecraft drift, flat field effects and geometric distortions. The UVIT observed fields of the sources are shown in Figs. 1 and 2. To investigate UV flux variability, we used the *Curvit* Python package (Joseph et al., 2021). We generated orbit-wise lightcurves from the combined Level 2 events list using the *curvit* function *curve_orbitwise()*, by extracting counts from a circular source region of radius 12 sub-pixels ($\sim 5''$). The extracted lightcurves were corrected for background, aperture effects, and saturation. The resulting fluxes were converted

to the total brightness values using the conversion factors provided in Table 11 of Tandon et al. (2020). In each light curve, we excluded photometric data points with uncertainties greater than twice the median error of all points in that light curve. The lightcurves are presented in Figs. 3, 4 and 5. The observed UV brightness values (not corrected for galactic extinction) of all the sources are given in Appendix.

3. Flux and Spectral Variability Analysis

3.1. Flux Variability

To characterize the flux variability of the sources, we computed the intrinsic variability amplitude, defined as the variance of the observed lightcurve after the removal of the measurement uncertainties (σ_m , in magnitudes; see Eq. 1). This was done following the methodology described by Ai et al. (2010).

$$\sigma_m = \sqrt{\Sigma^2 - \epsilon^2} \quad (1)$$

where, Σ^2 , the variance of observed magnitudes, is given by

$$\Sigma = \sqrt{\frac{1}{N-1} \sum_{i=1}^N (m_i - \langle m \rangle)^2} \quad (2)$$

and ϵ^2 , the mean error square due to measurement errors, is given by

$$\epsilon^2 = \frac{1}{N} \sum_{i=1}^N \epsilon_i^2 \quad (3)$$

Here, N and $\langle m \rangle$ are the number of orbits and the weighted mean of m_i measurements with the uncertainties ϵ_i , respectively. We considered a source to be variable only if $\Sigma^2 > \epsilon^2$, otherwise the intrinsic amplitude of flux variability $\sigma_m = 0$, and the source is non-variable.

We also calculated the fractional root mean square variability amplitude (F_{var}) to characterise flux variability. F_{var} is defined as (Vaughan et al., 2003)

$$F_{var} = \sqrt{\frac{S^2 - \overline{\sigma_{err}^2}}{\bar{x}^2}} \quad (4)$$

Here, S^2 is the sample variance of the light curve in counts/s, \bar{x} is the mean of the light curve and $\overline{\sigma_{err}^2}$ is the mean square error. They are defined as:

$$S^2 = \frac{1}{N-1} \sum_{i=1}^N (x_i - \bar{x})^2 \quad (5)$$

$$\overline{\sigma_{err}^2} = \frac{1}{N} \sum_{i=1}^N \sigma_{err,i}^2 \quad (6)$$

where x_i is the flux of individual data point in counts/s and $\sigma_{err,i}$ is the measured uncertainty on each data point. The error in F_{var} is defined as (Vaughan et al., 2003)

$$Err(F_{var}) = \sqrt{\left(\sqrt{\frac{1}{2N} \frac{\overline{\sigma_{err}^2}}{\bar{x}^2} F_{var}} \right)^2 + \left(\sqrt{\frac{\overline{\sigma_{err}^2}}{N} \frac{1}{\bar{x}}} \right)^2} \quad (7)$$

The flux variability results are presented in Table 3 for the sources that exhibit variability according to Eq. (1).

3.2. Spectral Variability

To investigate the spectral variability characteristics of the sources analysed in this work, we constructed colour magnitude diagrams (CMDs). In the optical band, the two subclasses of blazars are known to exhibit distinct trends in their CMDs: BL Lacs generally show a bluer-when-brighter (BWB) behaviour, whereas FSRQs tend to display a redder-when-brighter (RWB) trend (Negi et al., 2022; Li et al., 2024). In this study, we analyzed color variations for sources that have more than four simultaneous FUV and NUV photometric measurements on hour timescales. We fitted the CMDs of these sources using both unweighted and weighted linear least-squares fit methods. For the weighted linear least-squares fitting, which accounts for uncertainties in both the color index and magnitude, as well as their correlated errors, we employed two approaches, the Bivariate Correlated Errors and Intrinsic Scatter (BCES) method (Akritas and Bershady, 1996), and LINMIX_ERR, a Bayesian linear regression technique (Kelly, 2007). The fitting was performed using the following form: colour = slope \times (m - m_0) + intercept, where m_0 is the median of the magnitude values. The spectral fit plots are shown in Fig. 6 and the results of the fit are presented in Table 4 and Table 5. A positive slope in the CMD indicates a BWB trend, while a negative slope corresponds to a RWB trend. In addition, we considered a source to exhibit significant spectral variability if the absolute value of the linear correlation coefficient satisfies $|R| > 0.5$ and the probability of no correlation $P < 0.05$.

4. Notes on individual sources

4.1. 1ES 0120+340

The source 1ES 0120+340, located at a redshift of $z = 0.272$ (Costamante et al., 2001), is classified as a HSP BL Lac object (Goswami et al., 2024; Ackermann et al., 2015). It has previously been investigated for high-energy γ -ray emission by De La Calle Perez et al. (2003). In the present work, we report UV variability on hour timescales for the first time for this source. The source was observed during a single epoch using the FUV F154W filter and it exhibited statistically significant UV flux variability, confirming its intrinsically variable nature.

Table 1: Information of the sources studied in this work. The details of the sources are from Ackermann et al. (2015) except for the redshift of 1H 1720+117 which is from <https://simbad.u-strasbg.fr/simbad/sim-fbasic>. All the sources are detected in γ -rays by *Fermi*-LAT.

Name	RA (2000) (hh:mm:ss)	Dec (2000) (dd:mm:ss)	Optical type	SED type	z	M_{BH} (M_{\odot})	References for M_{BH}
1ES 0120+340	01:23:08.55	+34:20:47.40	BL Lac	HSP	0.272	1.0×10^9	Goswami et al. (2024)
1ES 0229+200	02:32:48.61	+20:17:17.47	BL Lac	HSP	0.139	4.8×10^8	Woo et al. (2005)
AO 0235+164	02:38:38.93	+16:36:59.27	BL Lac	LSP	0.940	$(4.7 \pm 2.0) \times 10^8$	Liu et al. (2006)
1H 0323+342	03:24:41.16	+34:10:45.85	NLSy1	HSP	0.063	$(2.8 - 7.9) \times 10^6$	Pan et al. (2018)
1ES 0347-121	03:49:23.17	-11:59:27.20	BL Lac	HSP	0.188	1.0×10^8	Woo et al. (2005)
PKS 0352-686	03:52:57.01	-68:31:18.59	BL Lac	HSP	0.087	-	-
PKS 0447-439	04:49:24.69	-43:50:08.96	BL Lac	HSP	0.205	6.0×10^8	Ghisellini et al. (2010b)
1H 0658+595	07:10:30.06	+59:08:20.36	BL Lac	HSP	0.125	1.8×10^8	Woo et al. (2005)
S5 0836+71	08:41:24.36	+70:53:42.17	FSRQ	LSP	2.218	5.0×10^9	Tagliaferri et al. (2015)
OJ 287	08:54:48.87	+20:06:30.64	BL Lac	LSP	0.306	1.8×10^{10}	Kuznetsov (2024)
Mrk 180	11:36:26.40	+70:09:27.30	BL Lac	HSP	0.045	1.7×10^8	Woo et al. (2005)
Ton 599	11:59:31.83	+29:14:43.82	FSRQ	LSP	0.725	1.0×10^8	Maurya et al. (2025)
4C +21.35	12:24:54.45	+21:22:46.38	FSRQ	LSP	0.435	6.0×10^8	Farina et al. (2012)
OQ 334	14:22:30.37	+32:23:10.44	FSRQ	LSP	0.682	3.9×10^8	Prince et al. (2021a)
Mrk 501	16:53:52.21	+39:45:36.60	BL Lac	HSP	0.034	4.2×10^8	Woo et al. (2005)
1H 1720+117	17:25:04.34	+11:52:15.47	BL Lac	HSP	0.018	-	-
S3 1741+19	17:43:57.83	+19:35:09.01	BL Lac	HSP	0.084	1.0×10^9	Goswami et al. (2024)
1ES 1959+650	19:59:59.85	+65:08:54.65	BL Lac	HSP	0.047	2.0×10^8	Ghisellini et al. (2010b)
PKS 2005-489	20:09:25.39	-48:49:53.72	BL Lac	HSP	0.071	5.0×10^8	Ghisellini et al. (2010b)
CTA 102	22:32:36.40	+11:43:50.90	FSRQ	LSP	1.037	8.5×10^8	Sahakyan (2020)
3C 454.3	22:53:57.74	+16:08:53.56	FSRQ	LSP	0.859	1.5×10^9	Sahakyan (2021)
1ES 2322-409	23:24:44.89	-40:40:43.89	BL Lac	HSP	0.174	1.0×10^9	Goswami et al. (2024)
1ES 2344+514	23:47:04.83	+51:42:17.88	BL Lac	HSP	0.044	5.5×10^8	Woo et al. (2005)
H 2356-309	23:59:07.90	-30:37:40.67	BL Lac	HSP	0.165	1.5×10^8	Woo et al. (2005)

Table 2: Log of observations. Here OBSID: Observation ID and MJD: Modified Julian Date

Name	Date of observation (dd-mm-yyyy)	OBSID	Filter	MJD Start	MJD End	Net exposure time (s)
1ES 0120+340	04-12-2018	A05_185T04_9000002548	F154W	58453.058824	58456.581583	64723
1ES 0229+200	22-09-2017	A03_078T01_9000001546	F154W	58017.831844	58018.174450	4889
			F172M	58018.176239	58018.674273	8724
			N219M	58017.831844	58018.246042	5787
			N245M	58018.310158	58018.467429	3703
			N263M	58018.469098	58018.674346	3453
	09-08-2021	T04_034T01_9000004632	F154W	59434.458958	59435.481634	14007
			F169M	59435.483371	59436.773205	15032
AO 0235+164	04-09-2016	G05_218T04_9000000640	F148W	57634.275091	57635.847420	22651
			N219M	57634.275042	57635.847469	22637
1H 0323+342	06-09-2020	T03_223T01_9000003850	F148W	59098.402173	59098.757547	8089
	30-09-2020	T03_236T01_9000003908	F148W	59122.499163	59122.765409	6579
	04-02-2022	A05_019T01_9000004906	F148W	59613.668914	59614.422499	9406
1ES 0347-121	21-08-2020	A07_146T01_9000003828	F148W	59082.304138	59082.519524	2942
PKS 0352-686	02-11-2018	A05_202T01_9000002484	F148W	58423.476028	58423.896043	11368
			F154W	58423.897781	58424.569960	11415
PKS 0447-439	15-12-2017	A04_082T01_9000001772	F154W	58102.012648	58102.544877	9956
			F169M	58102.546607	58102.562569	1360
			N245M	58102.012599	58102.544927	10031
			N263M	58102.546558	58102.562619	1367
1H 0658+595	19-11-2016	A02_085T02_9000000808	F154W	57711.076889	57711.427463	5556
			F172M	57711.440560	57711.706765	5995
			N245M	57711.437081	57711.571027	2874
			N263M	57711.577500	57711.588043	870
			N279N	57711.076839	57711.432454	4756
S5 0836+71	04-05-2017	G07_024T01_9000001206	F154W	57875.583540	57878.496745	58336
OJ 287	25-10-2020	T03_249T01_9000003934	F154W	59142.523770	59151.388587	52665
	18-11-2021	A10_067T01_9000004770	F154W	59535.873750	59536.902358	12262
	20-11-2021	A10_067T01_9000004774	F154W	59537.712823	59538.863612	11921
	18-04-2023	A12_104T02_9000005572	F154W	60051.025594	60052.712404	21125
Mrk 180	25-10-2018	A05_064T01_9000002450	F148W	58415.633992	58416.584151	10233
			F154W	58416.585873	58416.863542	4500
Ton 599	24-04-2020	T03_194T01_9000003620	F148W	58962.537295	58962.886370	7582
			F169M	58962.888109	58963.557386	9358
			F172M	58963.559120	58963.905821	9197
4C +21.35	25-04-2018	A04_219T01_9000002054	F148W	58233.540491	58233.609904	1902
			F172M	58233.611642	58233.891753	7434
OQ 334	12-01-2020	T03_175T01_9000003428	F148W	58859.704781	58859.979071	3823
			F154W	58859.980809	58860.518063	3788
			F169M	58860.519803	58860.793514	3818
			F172M	58860.795252	58860.798112	233
Mrk 501	25-03-2022	T05_015T01_9000005026	F154W	59662.314522	59664.496390	35246
	23-10-2022	A07_145T01_9000005370	F148W	59870.516163	59876.809498	19270
1H 1720+117	10-05-2018	A04_224T05_9000002088	F148W	58248.765601	58248.845706	2722
S3 1741+19	23-08-2019	A05_163T01_9000003118	F154W	58717.672011	58718.287319	7615
			F172M	58718.289059	58718.830209	9845

Table 2: Log of observations (continued)

Name	Date of observation (dd-mm-yyyy)	OBSID	Filter	MJD Start	MJD End	Net exposure time (s)
1ES 1959+650	05-10-2016	A02_199T01_9000000708	F154W	57666.211111	57666.358387	2989
			N263M	57666.211060	57666.358438	3016
	04-11-2016	G06_086T01_9000000774	F154W	57695.927007	57698.424637	16236
			N279N	57695.926935	57698.424604	16575
	16-11-2016	A02_199T01_9000000800	F154W	57708.444207	57708.452211	662
			N263M	57708.444207	57708.585130	2504
	25-10-2017	T01_200T01_9000001638	F154W	58051.181646	58051.875679	14906
			N279N	58051.181597	58051.875729	15000
PKS 2005–489	15-10-2019	A07_041T01_9000003234	F148W	58771.266239	58771.465491	2182
			F154W	58771.467225	58771.673344	3806
			F169M	58771.675082	58771.881982	3510
CTA 102	21-07-2017	G05_218T01_9000001394	F148W	57954.350649	57955.900967	31074
			N219M	57954.350598	57955.901018	27872
	07-08-2019	A05_160T01_9000003078	F148W	58702.177816	58702.383449	1924
			F154W	58702.385187	58702.395169	811
			F172M	58702.468388	58702.603028	3509
			F154W	58702.468388	58702.603028	9502
3C 454.3	20-10-2016	A02_149T01_9000000740	F154W	57680.625139	57681.323406	9502
			F172M	57681.325185	57681.752560	8068
			N219M	57680.625089	57681.323456	7683
			N279N	57681.325135	57681.752560	8111
	27-06-2023	T05_124T01_9000005712	F154W	60121.662641	60121.669951	595
			F169M	60121.671689	60121.809738	2855
			F172M	60121.811476	60122.548271	6035
			F148W	59033.450076	59033.664081	4296
1ES 2322–409	03-07-2020	A09_147T01_9000003754	F148W	59033.450076	59033.664081	4296
1ES 2344+514	22-10-2017	A04_049T01_9000001632	F172M	58048.015081	58048.285228	1876
			N245M	58047.952626	58048.285277	1797
	29-07-2021	A10_056T01_9000004598	F148W	59423.293892	59423.775796	11135
			F154W	59423.777535	59424.582497	10642
			F169M	59424.584238	59424.927427	5567
	06-08-2021	A10_056T01_9000004626	F148W	59431.677512	59432.358599	10791
			F154W	59432.360333	59432.764400	8178
			F169M	59432.909076	59433.052119	2087
			F154W	58407.368693	58408.794050	18452
H 2356–309	17-10-2018	A05_174T01_9000002440	F154W	58407.368693	58408.794050	18452
	18-10-2023	A05_174T01_9000005880	F154W	60234.470743	60235.833435	24817

Table 3: Flux variability analysis results for the sources that show variability. Here, N is the number of orbits, σ_m is the intrinsic amplitude of flux variability in magnitude, F_{var} is the fractional root mean square variability amplitude and $\text{Err}(F_{var})$ is the uncertainty in F_{var}

Name	Date (dd-mm-yyyy)	Filter	N	σ_m (mag)	F_{var} (counts/s)	$\text{Err}(F_{var})$ (counts/s)
1ES 0120+340	04-12-2018	F154W	44	0.022	0.022	0.031
1ES 0229+200	09-08-2021	F154W	14	0.036	-	-
1H 0323+342	04-02-2022	F148W	10	0.010	0.013	0.021
1ES 0347-121	21-08-2020	F148W	04	0.072	0.063	0.031
PKS 0447-439	15-12-2017	F154W	09	0.022	0.023	0.008
		N245M	09	0.010	0.007	0.005
1H 0658+595	19-11-2016	F172M	04	0.102	0.087	0.067
OJ 287	25-10-2020	F154W	85	0.054	0.053	0.005
		F154W	11	0.027	0.027	0.011
		F154W	16	0.055	0.052	0.012
Mrk 501	25-03-2022	F154W	30	0.015	0.017	0.003
		F148W	54	0.027	0.026	0.003
Mrk 180	25-10-2018	F148W	12	0.023	0.022	0.012
		F154W	05	0.023	0.022	0.020
Ton 599	24-04-2020	F148W	05	0.059	0.052	0.029
		F169M	11	0.168	0.145	0.025
		F172M	06	0.199	0.172	0.031
4C +21.35	25-04-2018	F148W	02	0.065	0.045	0.022
OQ 334	12-01-2020	F148W	05	0.121	0.116	0.008
		F154W	07	0.168	0.143	0.011
		F169M	05	0.099	0.097	0.012
S3 1741+19	23-08-2019	F154W	08	0.029	0.009	0.228
		F172M	08	0.167	0.171	0.048
1ES 1959+650	04-11-2016	F154W	18	0.040	0.039	0.004
		N279N	18	0.044	0.041	0.006
		F154W	11	0.014	0.016	0.005
PKS 2005-489	25-10-2017	N279N	11	0.046	0.041	0.005
		F169M	04	0.013	0.013	0.018
		F148W	21	0.062	0.058	0.010
CTA 102	21-07-2017	N219M	21	0.035	0.034	0.017
		F172M	02	0.247	0.220	0.052
3C 454.3	27-06-2023	F172M	08	0.078	0.062	0.072
1ES 2344+514	29-07-2021	F169M	05	0.062	0.054	0.047
		F148W	11	0.053	0.041	0.042

Table 4: Spectral variability results determined using the unweighted linear least-squares fitting method. Here, R is the linear correlation coefficient and P is the probability for no correlation.

Name of source	OBSID	N	color/mag	Slope	Intercept	R	P
PKS 0447-439	A04_082T01_9000001772	09	(F154W-N245M)/F154W	0.91±0.16	0.54±0.01	0.91	0.00
1ES 1959+650	G06_086T01_9000000774	18	(F154W-N279N)/F154W	0.34±0.23	0.82±0.01	0.35	0.16
	T01_200T01_9000001638	11	(F154W-N279N)/F154W	-0.61±0.51	0.73±0.01	-0.37	0.26
CTA 102	G05_218T01_9000001394	21	(F148W-N219M)/F148W	0.73±0.20	0.90±0.02	0.65	0.00

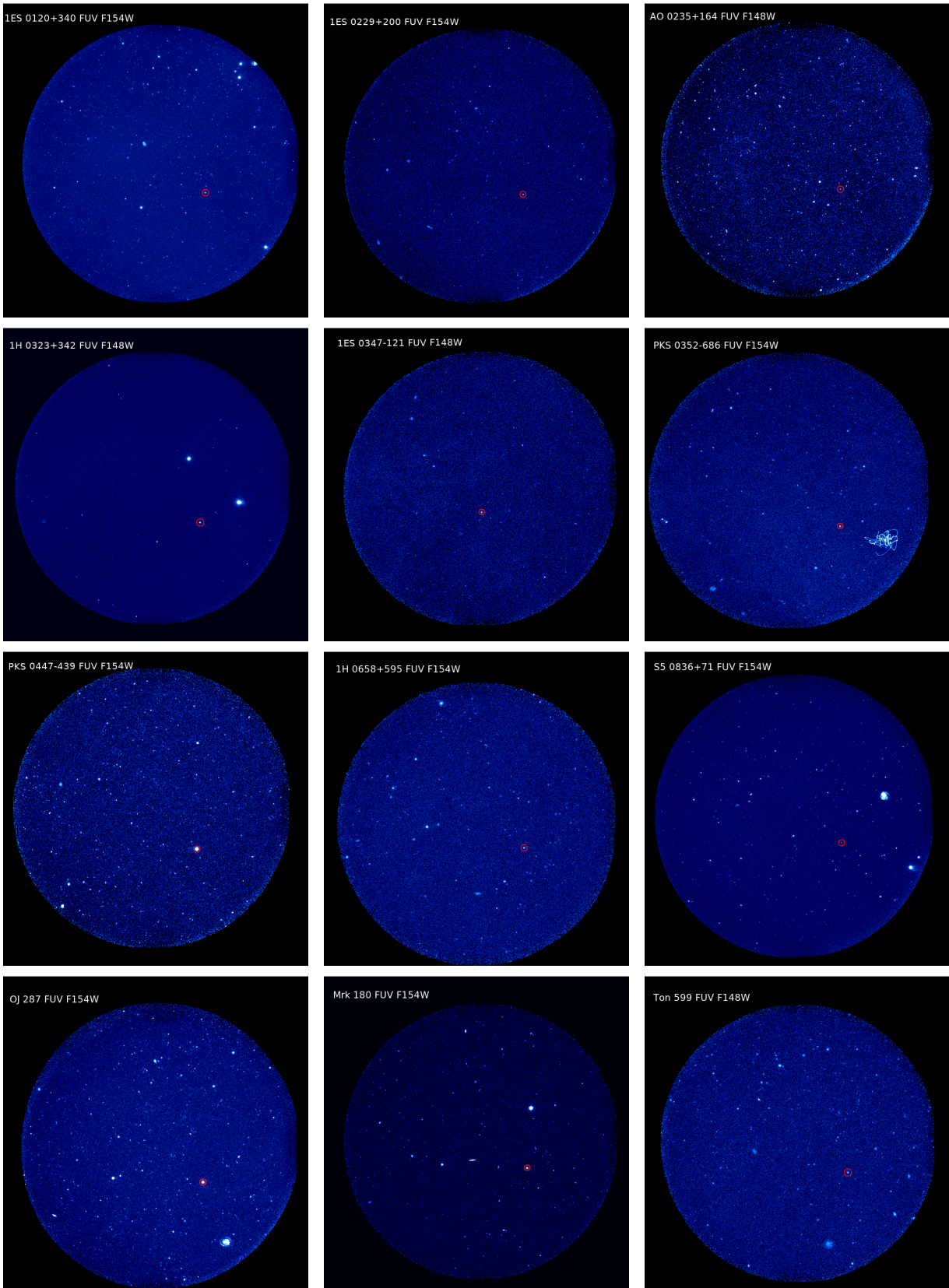


Figure 1: FUV field images of the blazar sources analyzed in this work. Red circles in each field image shows the target sources. The source name and the respective filter name are shown in all the field images. The field of view of each image is $\sim 28'$ diameter. In the field image of PKS 0352–686, the pattern observed near the target source is due to an unmasked hot pixel showing the drift correction patterns.

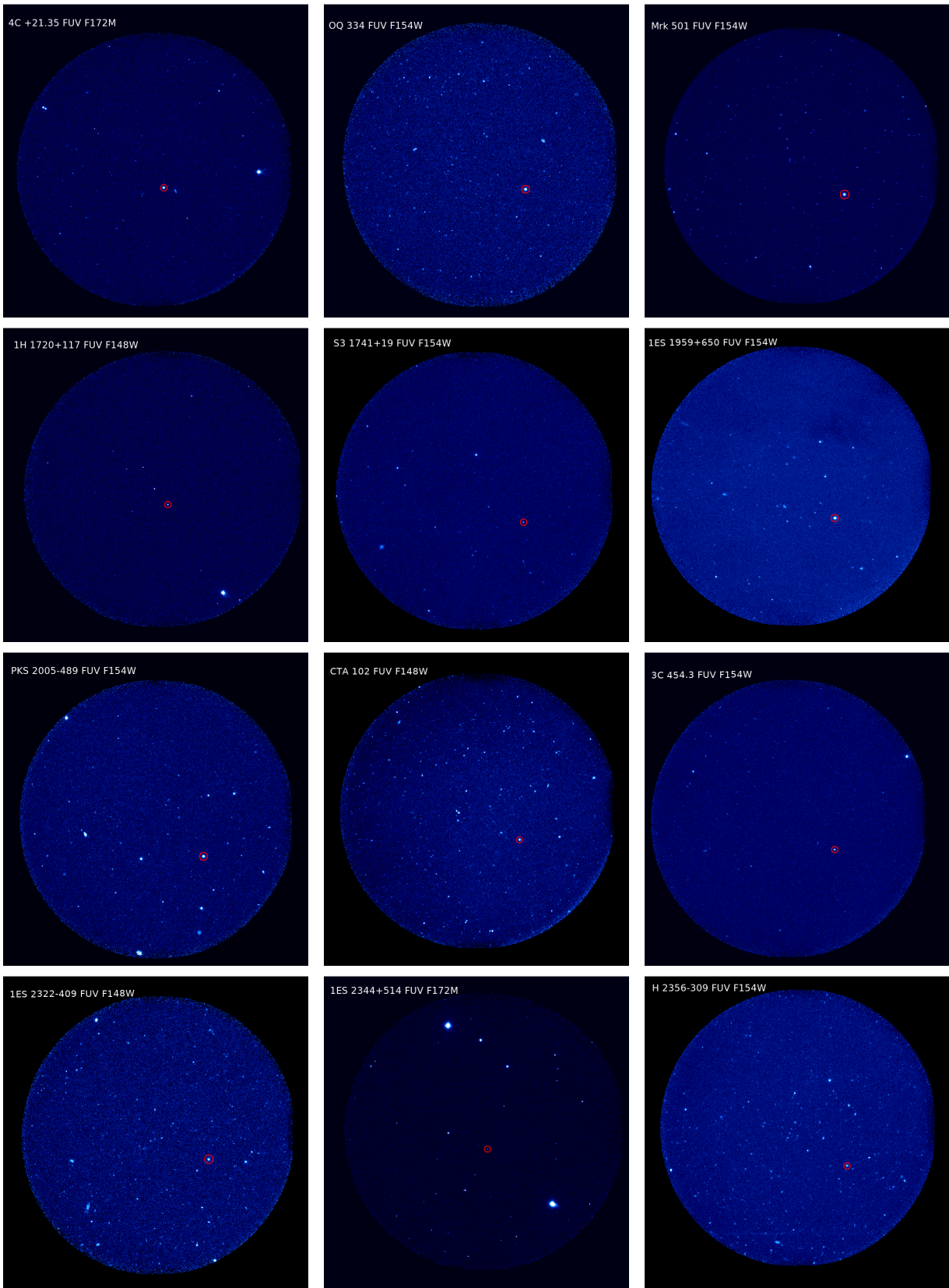


Figure 2: FUV field images of the blazar sources analyzed in this work. Red circles in each field image shows the target sources. The source name and the respective filter name are shown in all the field images. The field of view of each image is $\sim 28'$ diameter.

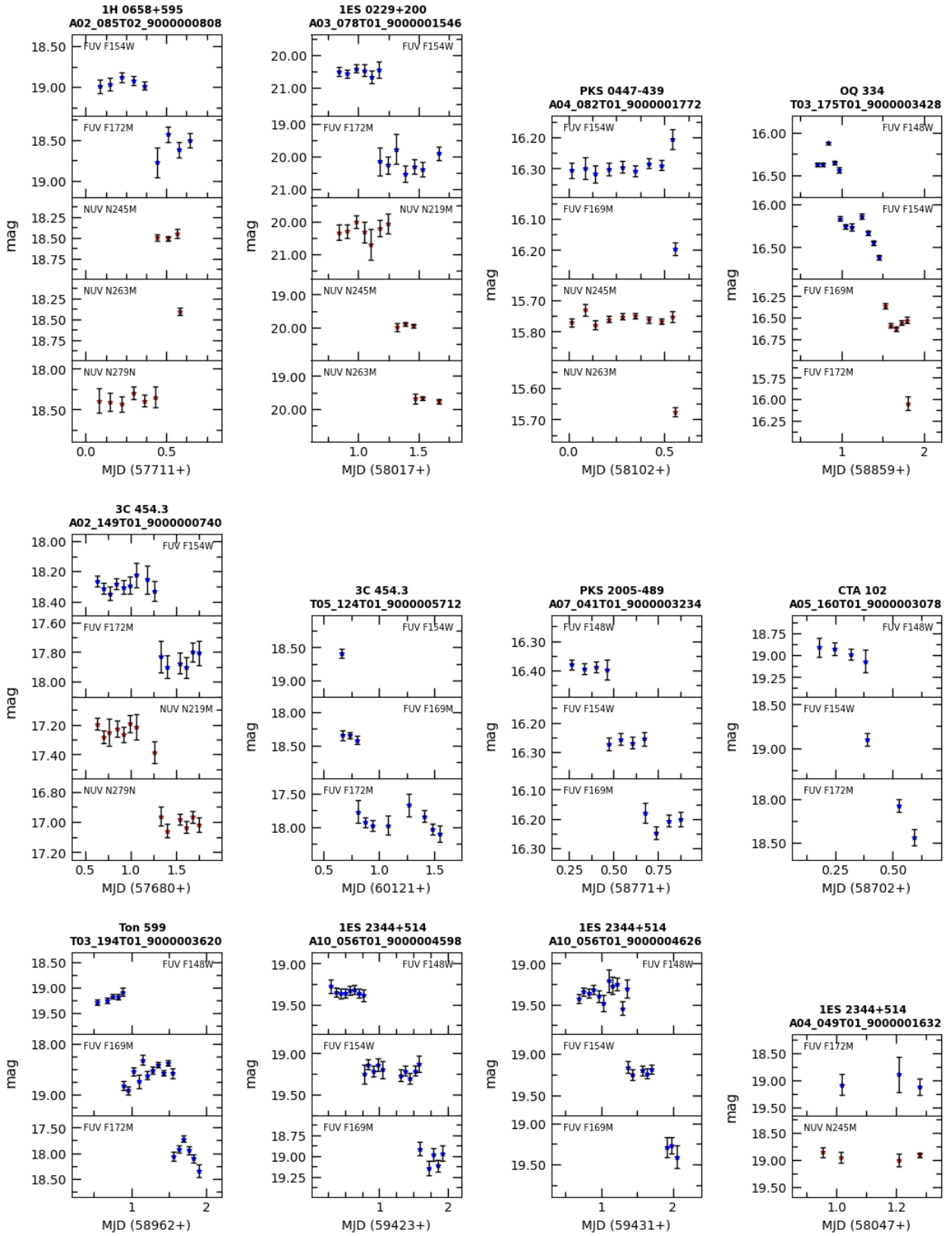


Figure 3: FUV (blue stars) and NUV (brown stars) lightcurves of sources. The source name along with the observation ID and filter names are provided in the respective plots.

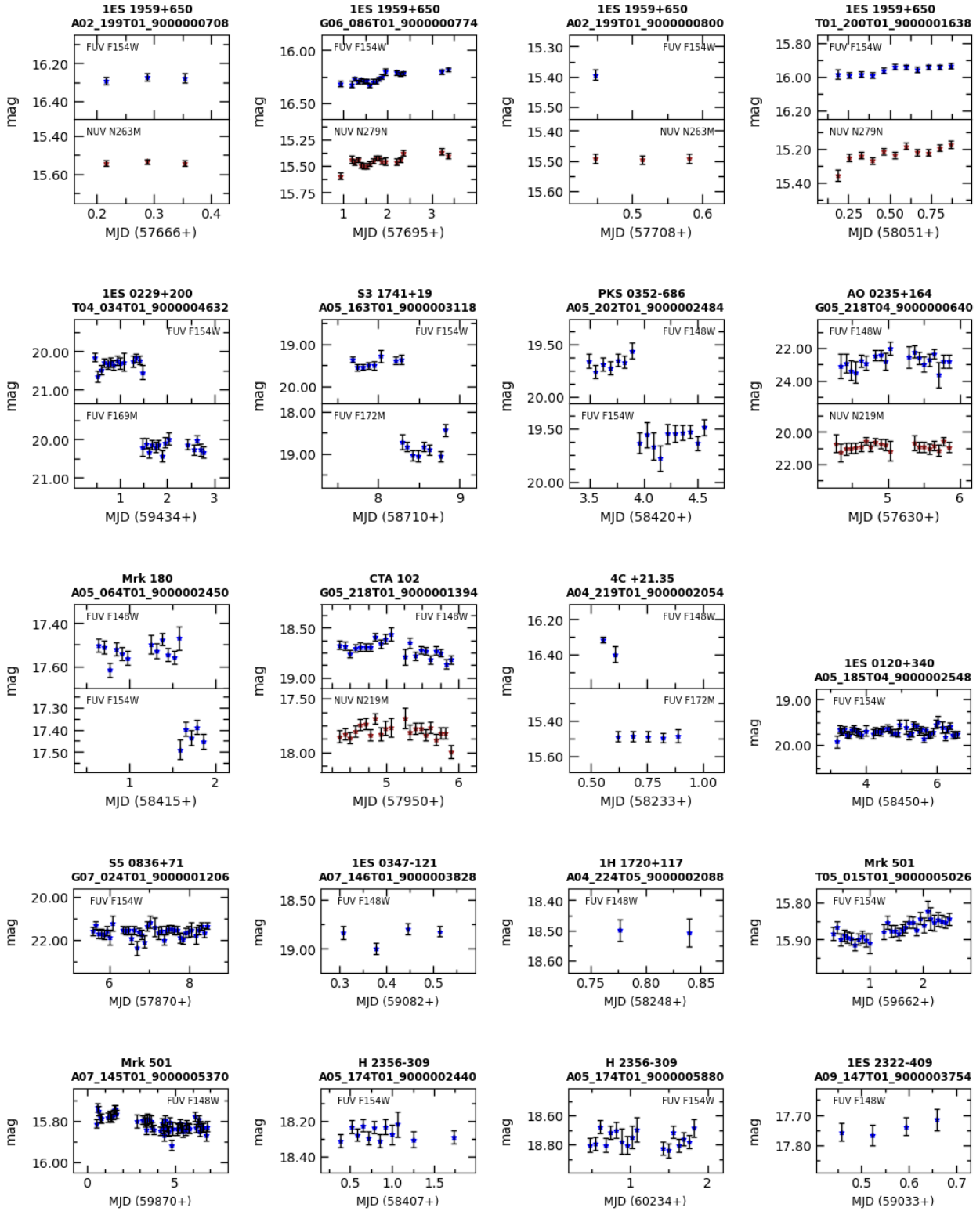


Figure 4: FUV (blue stars) and NUV (brown stars) lightcurves of sources. The source name along with the observation ID and filter names are provided in the respective plots.

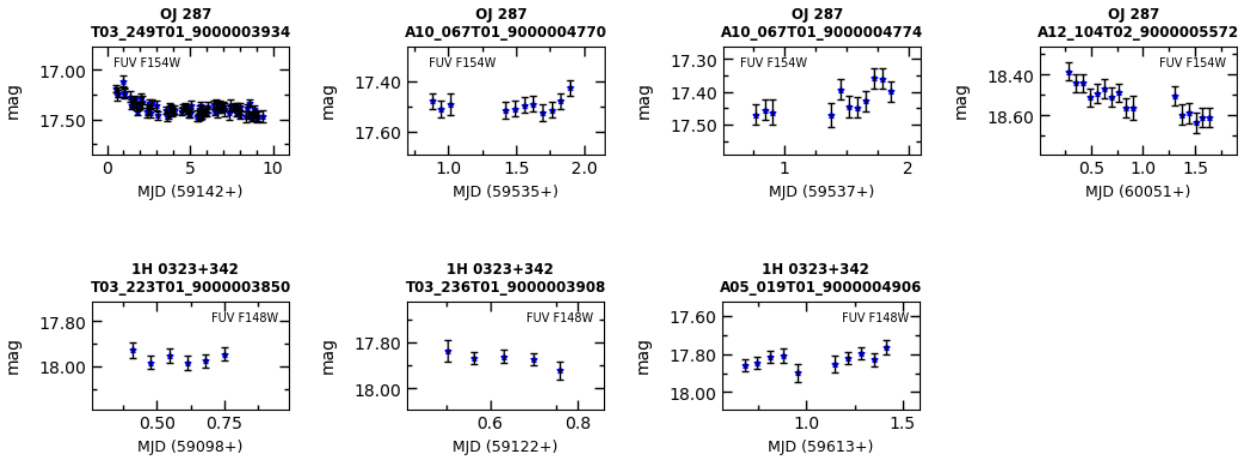


Figure 5: FUV (blue stars) lightcurves of sources. The source name along with the observation ID and filter names are provided in the respective plots.

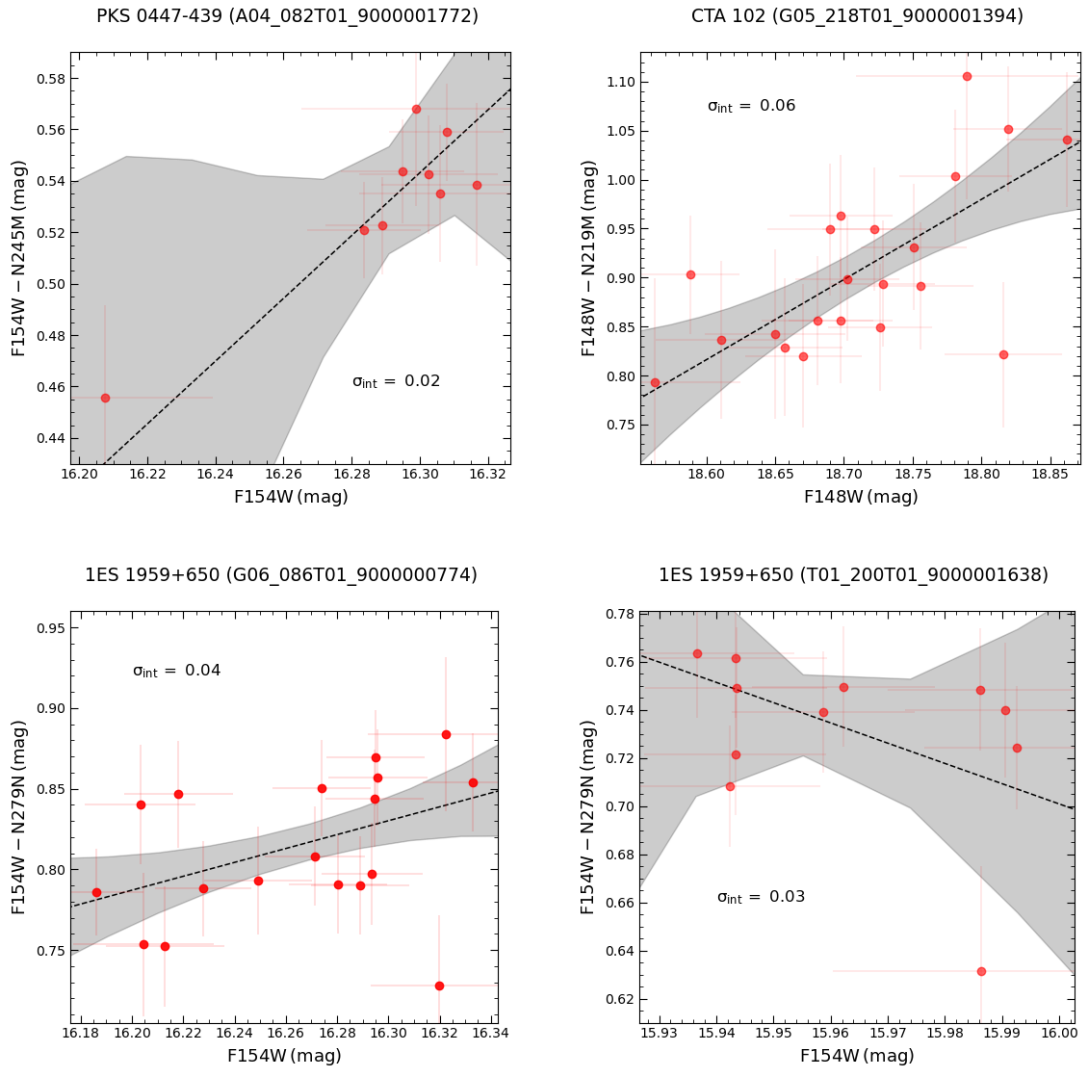


Figure 6: The CMDs of the sources analyzed for spectral variability. The black dashed line and the grey shaded region represent the best fit and uncertainty range on the fit from Bayesian analysis using LINMIX_ERR method. The intrinsic scatter (σ_{int}) value is provided in each plot and the name of the source along with the OBSID is provided on the top of each plot (also refer Table 4 and 5).

Table 5: Spectral variability results determined using the BCES and Bayesian methods. Here, Columns 5 and 6 are the slope and intercept values along with their associated errors calculated based on BCES method, Column 7 and 8 are the slope and intercept values along with their associated errors calculated based on Bayesian method.

Name	OBSID	N	color/mag	BCES		Bayesian	
				Slope	Intercept	Slope	Intercept
PKS 0447–439	A04_082T01_9000001772	09	(F154W–N245M)/F154W	0.91±0.09	0.54±0.01	1.08±4.00	0.54±0.04
1ES 1959+650	G06_086T01_9000000774	18	(F154W–N279N)/F154W	0.55±0.24	0.82±0.01	0.44±0.32	0.82±0.01
	T01_200T01_9000001638	11	(F154W–N279N)/F154W	–1.73±1.41	0.74±0.02	–0.54±8.01	0.73±0.03
CTA 102	G05_218T01_9000001394	21	(F148W–N219M)/F148W	0.78±0.19	0.90±0.01	0.80±0.40	0.90±0.02

4.2. IES 0229+200

IES 0229+200 is a HSP BL Lac object with a TeV spectrum extending up to 10 TeV (Aharonian et al., 2007b) and located at a redshift of $z = 0.139$ (Ackermann et al., 2015). Modest optical variability of ~ 0.2 mag was reported by Wierzcholska et al. (2015) based on monitoring observations during 2007 - 2012. It was found to be variable in X-rays from NuSTAR observations (Pandey et al., 2017). It was found to show rapid intra-night optical variability (Bachev et al., 2012), and a rapid optical flare lasting for about 6 hours was reported by Kishore et al. (2024). The UV flux variability in this source was first investigated by Reshma et al. (2024). In this work, we re-investigated its UV flux variability using observations from two additional epochs. The source was found to exhibit variability only in the F154W filter during the 2021 epoch.

4.3. AO 0235+164

AO 0235+164 is a LSP BL Lac object located at a redshift of $z = 0.94$ (Ackermann et al., 2015). Raiteri et al. (2001) systematically investigated the source in the radio and optical bands and reported quasi-periodic oscillations with the possible indication of the source to host a binary black hole system (Romero et al., 2003). Although it is typically classified as a BL Lac object, the source also exhibits several characteristics commonly associated with FSRQs (Wang and Jiang, 2020). AO 0235+164 is well known as an optically violent variable source (Roy et al., 2023) and its long-term, multi-wavelength variability, has been studied extensively by Vlasyuk et al. (2024). It has been extensively studied for variability across wavelengths and has been found to show flux variations on a range of timescales (Romero et al., 2000; Raiteri et al., 2001; Ackermann et al., 2012). This source was observed simultaneously in the FUV and NUV bands on 4 September 2016. During this epoch the source did not show variability in either the FUV or NUV bands.

4.4. 1H 0323+342

1H 0323+342 was first discovered in the *HEAO-1* survey by Wood et al. (1984). It is a radio-loud NLSy1 galaxy, notable for being one of the nearest ($z = 0.063$) and optically brightest members of this class as well as one of the few radio-loud NLSy1 galaxies detected at γ -ray energies (Turner et al., 2022). Radio-loud NLSy1 galaxies are known to share several observational properties with blazars (Abdo et al., 2009b). The source

hosts a central black hole with an estimated mass of $\sim 10^7 M_{\odot}$ (Zhou et al., 2007). The source was found to be variable on intra-night time scales in the optical band (Paliya et al., 2013, 2014; Ojha et al., 2019). Feigelson et al. (1986) reported rapid variability in the X-ray band with a halving timescale of 30 seconds. From long term variability analysis using observations from *Swift*, D’Ammando (2020a) found correlated variations in the optical, UV and X-ray bands favouring the contribution of the jet to the observed emission in those bands. This source was observed with UVIT over three epochs in the FUV band using the F148W filter. Of these three epochs, significant UV flux variabilities were detected during the observations carried out on 4 February 2022, representing the first report of UV variability on this source.

4.5. IES 0347–121

IES 0347–121 located at a redshift of $z = 0.188$ (Woo et al., 2005) is a member of the Einstein Slew Survey (Elvis et al., 1992) and was classified as a BL Lac object by Schachter et al. (1993). The source is also known to be an extreme TeV blazar (Goswami et al., 2024). Its X-ray flux and spectral variability have previously been studied by Pandey et al. (2018) and was found to be non-variable in X-rays. The source was found to be variable in the optical from long term monitoring observations (Wierzcholska et al., 2015). In this work, we report, for the first time, UV variability in this source on timescales of hours. The source was observed on 21 August 2022 in the FUV band and was found to be variable.

4.6. PKS 0352–686

PKS 0352–686 is a BL Lac type blazar located at a redshift of $z = 0.087$ (Masetti et al., 2006). From observations carried out with the Transiting Exoplanet Survey Satellite, Tripathi et al. (2026) reported detection of quasi-periodic oscillation in this source. UV observations of this source carried out in 2018 using two FUV filters revealed no significant variability during that epoch.

4.7. PKS 0447–439

PKS 0447–439 is a BL Lac type blazar (Muriel et al., 2015) located at a redshift of $z = 0.205$ (Perlman et al., 1998). The source was originally discovered in the radio band by Large et al. (1981) and has since been extensively observed across

multiple wavelengths, including radio (Gregory et al., 1994), X-rays (White et al., 1994), UV (Lampton et al., 1997), and high-energy γ -rays by *Fermi*-LAT (Abdo et al., 2009a). It is believed to be powered by a supermassive black hole with a mass of approximately $6 \times 10^8 M_{\odot}$ (Ghisellini et al., 2010b). In this work, we report for the first time the detection of UV variability in PKS 0447–439 on hour timescales. It was observed on 15 December 2017, during which variability was detected in both the F154W and N245M filters.

4.8. 1H 0658+595

1H 0658+595 ($z = 0.125$) is classified as a HSP blazar and is known to be an extreme TeV emitter (Furniss et al., 2013). A long-term investigation of its X-ray and γ -ray variability by Goswami et al. (2024) revealed significant flux and spectral variations, with X-ray variability observed on timescales ranging from days to weeks. In this work, we searched for UV flux variability on hour timescales, however, the source was found to be variable only in the F172M observation.

4.9. S5 0836+71

S5 0836+71, is a FSRQ (Malizia et al., 2000) located at a high redshift of $z = 2.218$ (Ackermann et al., 2015). It is classified as a low-polarization quasar in the optical band (Impey and Tapia, 1990), and is known to host a supermassive black hole with a mass of $3 \times 10^9 M_{\odot}$ (Ghisellini et al., 2010a) and $5 \times 10^9 M_{\odot}$ (Tagliaferri et al., 2015). The source exhibits a prominent big blue bump in its SED indicative of strong thermal emission from the accretion disk (Raiteri et al., 2014, 2019). Orienti et al. (2020) investigated the polarisation and multi-wavelength variability of S5 0836+71 from radio to γ -rays using VLBA, *Swift* and *Fermi*-LAT observations and reported that the optical-UV emission was largely dominated by the accretion disk exhibiting lesser variability. In this study, we examined the source’s UV flux variability on hour timescales using UVIT observations obtained on 4 May 2017. No variability was detected during this epoch.

4.10. OJ 287

OJ 287 is a LSP BL Lac type blazar at a redshift of $z = 0.306$. It is a well-known blazar to host a binary supermassive black hole (Sillanpaa et al., 1988) detected with a high optical activity at a periodic interval of 12 years (Prince et al., 2021b). OJ 287 is detected in TeV (O’Brien, 2017) and has been extensively studied for variability across wavelengths. It has been found to show X-ray flux and spectral variations (Zhou et al., 2024). It is variable in the optical with Kishore et al. (2024) reporting a shortest variability time scale of 0.38 days. It has also been found to be variable in infra-red (Gupta et al., 2022), as well as in the optical and γ -ray bands (Rajput et al., 2021). In addition to the detailed UV flux variability analysis reported by Reshma et al. (2024), we analyzed four new epochs of observations carried out with UVIT in this work. We found the source to show UV flux variability on three epochs of observations.

4.11. Mrk 180

Mrk 180 is a HSP blazar located at a redshift of $z = 0.045$. It was first identified as a BL Lac type object in 1976 (Mondal et al., 2023). It was initially detected in X-rays by Hutter and Mufson (1981), and its very high energy TeV γ -ray emission was subsequently discovered by Albert et al. (2006). Its optical long term variability has been analysed by Nilsson et al. (2018). Mrk 180 was observed by UVIT on 25 October 2018, using two FUV filters, F148W and F154W. We found the source to be variable in both the filters.

4.12. Ton 599

Ton 599 is a LSP FSRQ located at a redshift of $z = 0.725$ (Rajput et al., 2024) and it is a TeV γ -ray source (Mirzoyan, 2017). The source is classified as both an optically violent variable and a highly polarized quasar (Patel et al., 2018). It exhibits variability across a broad energy range, from radio to γ -rays, and has been the subject of extensive flux variability studies for more than three decades (Manzoor et al., 2024). A multiwavelength variability study conducted by Prince (2019) during the 2017 high-activity state reported strong γ -ray variability and a comparatively less variability in the X-ray band. It was found to show strong optical flux variations (Vince et al., 2025). It was found to show correlated optical and GeV flux variations at certain epochs, while such correlated variations are not seen at all times (Rajput et al., 2024). In this work, we analyzed UVIT observations of Ton 599 obtained on 24 April 2022, using three different FUV filters. UV flux variability was detected in all the three filters.

4.13. 4C +21.35

4C +21.35 is FSRQ type blazar located at a redshift of $z = 0.435$ (Ackermann et al., 2015). It is a well known γ -ray emitting source (Hartman et al., 1999), and hosts a central black hole with an estimated mass of $\sim 6 \times 10^8 M_{\odot}$ (Farina et al., 2012). It has been analysed for X-ray flux variation by Wiercholska and Wagner (2016). Outburst in the GeV band was reported by Donato (2010), and in the high energy γ -ray band flux variations with a doubling time scale of about 10 minutes was reported by Aleksić et al. (2011). The broadband SED of the source has been studied in detail by Ackermann et al. (2014). The source was observed with UVIT on 25 April 2018 using two FUV filters, F148W and F172M. UV variability was detected in the F148W filter.

4.14. OQ 334

OQ 334, is a FSRQ located at a redshift of $z = 0.682$. It is a very high energy γ -ray source detected by the *Fermi*-LAT (D’Ammando et al., 2021). Multi-wavelength studies, covering radio to very high energy γ -rays have been carried out on this source (D’Ammando et al., 2021; Ren et al., 2024). Until 2018, OQ 334 remained largely in a quiescent state (Abdollahi et al., 2020), after which it underwent a series of flaring episodes accompanied by significant changes in its broad emission lines.

These spectral transformations led Mishra et al. (2021) to classify the source as a changing-look type blazar, owing to its transition between FSRQ and BL Lac characteristics. It was also found to show repeated flaring activity in the GeV γ -ray band (Ciprini and Cheung, 2020). In this work, we investigated hour UV variability in OQ 334 for the first time. UVIT observations carried out on 12 January 2020, using four different FUV filters revealed significant variability in three of them, indicating a variable nature in the UV band.

4.15. Mrk 501

Mrk 501 is a HSP BL Lac object at a redshift of $z = 0.034$. It has been studied for optical/UV and X-ray variability on timescales ranging from months to years by Kapanadze et al. (2023) and Tantry et al. (2024). Long term variability study in the X-ray and γ -ray band was studied by Gliozzi et al. (2006). Rapid optical variability on minutes timescale was reported by Zeng et al. (2019). It has been extensively studied for UV variability on hour timescales by Reshma et al. (2024). In 2022, UVIT observed the source during two separate epochs using different FUV filters, and UV variability was detected in both observations.

4.16. 1H 1720+117

1H 1720+117, located at redshift $z = 0.018$, is classified as a BL Lac type blazar. Nieppola et al. (2006) categorized it as an ISP blazar, with a synchrotron peak frequency at $\nu_s = 6.3 \times 10^{15}$ Hz. Optical monitoring by Kalita et al. (2021) reported no intraday variability in its lightcurve. Interestingly, despite its BL Lac classification, the source exhibited a pronounced RWB trend in the optical band. During UVIT observations carried out on 10 May 2018 using the FUV filter F148W, the source was found to be non-variable.

4.17. S3 1741+19

S3 1741+19, identified in the *Einstein* Slew Survey (Perlman et al., 1996), is a HSP blazar located at a redshift of $z = 0.084$. It is hosted by one of the largest and most luminous elliptical host galaxies among BL Lac objects. The host galaxy appears to have been tidally distorted due to interactions with two companion galaxies, forming a dynamically interacting triplet system (Abeysekara et al., 2016; Ahnen et al., 2017). The source was detected in the high-energy MeV γ -ray regime by *Fermi*-LAT (Abdo et al., 2010b), while its very-high-energy γ -ray emission was first reported by Berger (2011). Optical observations by Heidt et al. (1999) provided an early detailed study of the source, and Abeysekara et al. (2016) reported variability in both the optical and UV bands. In contrast, Goswami et al. (2024) found no significant variability in the optical and γ -ray bands, but reported clear variability at X-ray energies. On 23 August 2019, UVIT observed S3 1741+19 using two FUV filters, F154W and F172M. We detected UV variations on hour timescales in both the filters.

4.18. 1ES 1959+650

The blazar 1ES 1959+650 was first detected in the X-ray band by the *Einstein* Slew Survey (Elvis et al., 1992) and subsequently classified as a BL Lac object by Schachter et al. (1993). Located at a redshift of $z = 0.047$, it is categorized as a HSP blazar (Krawczynski et al., 2004). The source is a known γ -ray emitter, with its first detection in the TeV regime reported by Nishiyama (1999), followed by detailed studies of a TeV outburst observed with VERITAS (Holder et al., 2002). A multi-wavelength variability analysis was presented by Aliu et al. (2014). In this work, we investigated the UV variability on hour timescales using four epochs of observations with UVIT. We observed flux variations in both FUV and NUV during two epochs, namely 4 November 2016 and 25 October 2017. However, we found no statistically significant spectral variations on both the epochs.

4.19. PKS 2005–489

PKS 2005–489 was first identified as a radio source in the Parkes 2.7 GHz survey by Wall et al. (1975) and later classified as a BL Lac object at a redshift of $z = 0.071$ (Wall et al., 1986; Falomo et al., 1987). It is recognized as a HSP blazar (Acero et al., 2010). Spectral variability in the X-ray band was studied by Perlman et al. (1999), while Dominici et al. (2004) investigated its long-term optical variability. The H.E.S.S. Cherenkov telescope array reported the first detection of very-high-energy γ -ray emission from the source (Aharonian et al., 2005). During a UVIT observation on 15 October 2019, the source was monitored using three FUV filters. Variability was detected only in the F169M filter.

4.20. CTA 102

CTA 102, located at a redshift of $z = 1.037$, is classified as a FSRQ (Schmidt, 1965) and hosts a central black hole with a mass $8.5 \times 10^8 M_\odot$ (Zamaninasab et al., 2014). It is also categorized as a highly polarized quasar, exhibiting optical polarization levels exceeding 3% (Moore and Stockman, 1981). The source has been studied for long-term flux and spectral variability across multiple wavelengths, including radio, optical–UV, X-rays, and γ -rays (D’Ammando et al., 2019). CTA 102 is notable for being the third known FSRQ to display extremely rapid γ -ray flux variability on timescales of only a few minutes (Shukla et al., 2018). The source was observed with UVIT during two epochs, on 21 July 2017 and 7 August 2019. Significant UV flux variability was detected on both the epochs. Additionally, during the epoch with simultaneous FUV and NUV observations, we detected spectral variations characterized by a significant BWB trend.

4.21. 3C 454.3

3C 454.3, located at a redshift of $z = 0.859$, is a well-known and highly variable FSRQ hosting a central black hole with a mass of about $1.5 \times 10^9 M_\odot$ (Sahakyan, 2021). The source is known for its dramatic variability across the entire electromagnetic spectrum. Its multi-wavelength behaviour has been extensively investigated over the past decades (Raiteri et al., 2008b;

Jorstad et al., 2013; Amaya-Almazán et al., 2020; Chen et al., 2025). We examined hour timescale UV variability using UVIT observations carried out on 20 October 2016 and 27 June 2023. UV variability was detected during the 2023 epoch, while no variability was observed in the 2016 data.

4.22. 1ES 2322–409

1ES 2322–409 is classified as a BL Lac object based on its featureless optical spectrum (Thomas et al., 1998). Although its redshift remains uncertain, Jones et al. (2009) reported a value of $z = 0.174$. Based on its synchrotron peak located at $10^{15.92}$ Hz, the source is characterized as a HSP blazar (Ackermann et al., 2015). It is a bright TeV emitter, with its very-high-energy γ -ray emission first reported by Abdalla et al. (2019). UVIT observations of 1ES 2322–409 were carried out on 3 July 2020. The source was found to be non-variable during this epoch.

4.23. 1ES 2344+514

1ES 2344+514 is a BL Lac object located at a redshift of $z = 0.044$. It is found to be variable in X-rays (Devanand et al., 2022). Optical variability of the source was studied by Gaur et al. (2012) and Cai et al. (2022). Abe et al. (2024) reported long timescale UV variability using *Swift*-UVOT observations. Its UV variability has been studied in detail by Reshma et al. (2024), who reported hour timescale flux variations in the UV band. In the present work, we further examined the source for variability using three additional epochs of UVIT observations conducted on 22 October 2017, 29 July 2021 and 8 August 2021. The source was found to be variable on two of the three epochs analyzed here.

4.24. H 2356–309

The BL Lac object H 2356–309 is hosted by an elliptical galaxy at a redshift of $z = 0.165$ (Falomo, 1991). It is classified as a HSP blazar, originally identified in the optical band by Schwartz et al. (1989). The source was first detected in X-rays by the *UHURU* satellite, followed by observations with HEAO-I (Forman et al., 1978; Wood et al., 1984). Its very-high-energy γ -ray emission has been studied using the H.E.S.S. Cherenkov telescope (Aharonian et al., 2006). Wani and Gaur (2020) investigated its flux and spectral variability in the X-ray regime. The source was observed for UV variability on 17 October 2018 and 18 October 2023. Variability was not detected in the source on both the epochs of observations.

5. Results and Discussion

Of the 24 sources analyzed for flux variability, 18 exhibited significant variability, while 6 showed no detectable variations. Among the 18 variable sources, 15 have observations only in the FUV band, whereas three have simultaneous observations in both the FUV and NUV bands. In the NUV band, the variability amplitude ranges from 0.010 mag to 0.046 mag, while in the FUV band it spans a wider range, from 0.010 mag to 0.247 mag. For two of the three sources with simultaneous FUV and NUV

observations, the variability amplitude is larger in the FUV than in the NUV. The flux variability results for the variable sources are presented in Table 3. The UV lightcurves of the sources analyzed in this work are shown in Figs. 3, 4, and 5.

The low energy hump in the broadband SED of FSRQs (covering radio, infrared, optical and UV wavelengths), and BL Lacs (extending from infrared through optical and UV to X-rays) is dominated by synchrotron emission from relativistic non-thermal electrons in their jets. However, in FSRQs during their faint states, prominent contribution from accretion disk is evident in the low-energy hump of the SED (Paliya et al., 2016, 2017). Similarly, BL Lacs may also exhibit signatures of accretion disk emission during low states (Raiteri et al., 2008a). Consequently, the observed UV emission in both FSRQs (with broad emission lines and radiatively efficient accretion disks) and BL Lacs (with weak or absent emission lines and radiatively inefficient accretion disks) is likely a combination of jet and accretion disk emission. Since thermal emission from the accretion disk has a bluer spectral shape, while non-thermal synchrotron emission has a redder spectral shape, the observed colour variations in blazars are governed by changes in the disk emission, jet emission or both. In the optical band, FSRQs are generally known to exhibit a RWB trend (Bonning et al., 2012; Sarkar et al., 2019), whereas BL Lacs typically show a BWB behaviour (D’Amicis et al., 2002; Vagnetti et al., 2003; Fiorucci et al., 2004; Meng et al., 2018; Gaur et al., 2019). However, sources are also known to exhibit both BWB and RWB trends (Wu et al., 2011; Rajput et al., 2019).

In our sample, constrained by the availability of simultaneous FUV and NUV observations, UV colour variability could be examined only for three sources, namely CTA 102 (FSRQ), PKS 0447–439 and 1ES 1959+650 (both BL Lacs). For 1ES 1959+650, during the observations on 4 November 2016, we found a weak positive correlation ($R = 0.35$), however, this correlation is not statistically significant ($P = 0.16$) and the fitted slope (0.34 ± 0.23) is consistent with zero. The slopes from BCES and LINMIX_ERR too are consistent with zero (see Table 5). During the observations on 24 October 2017, we found a weak negative correlation ($R = -0.37$), which is again statistically insignificant ($P = 0.26$). Thus, no significant colour variability was detected in 1ES 1959+650. In contrast, in both PKS 0447–439 and CTA 102, we found a statistically significant positive correlation between UV colour and magnitude (with R of 0.91 in PKS 0447–439 and 0.65 in CTA 102, and $P < 0.01$ in both the sources) indicating a clear BWB trend. Both sources showed mild UV brightening during the epochs in which colour variations were detected. The observed CMDs along with the fits are shown in Fig. 6. The results of the fit are given in Tables 4 and 5.

During the epoch of the UVIT observations of CTA 102, the source was in a relatively bright γ -ray flux state (within ± 3 days of UVIT observations) with *Fermi*-LAT flux values² in the range $(1.6\text{--}1.8) \times 10^{-6}$ photons $\text{cm}^{-2} \text{s}^{-1}$. In contrast, PKS

²<https://fermi.gsfc.nasa.gov/ssc/data/access/lat/LightCurveRepository>

0447–439 was not detected in γ -rays by *Fermi* within ± 3 days of the UVIT observations. Irrespective of their γ -ray brightness, the observed UV brightening in both the sources may be attributed to fresh acceleration of electrons to higher energies as expected in shock in-jet models (Marscher and Gear, 1985; Kirk et al., 1998). Also, magnetic reconnection events or localized turbulence in the jet can lead to enhanced emission at shorter (bluer) wavelengths leading to the observed BWB trend. Changes in the Doppler factor due to geometrical effects, such as variations in the viewing angle of a curved or inhomogeneous jet could also lead to a BWB behaviour (Villata et al., 2004; Papadakis et al., 2007).

A similar UV colour variability analysis by Reshma et al. (2024) reported BWB trends in four BL Lacs and one FSRQ. This suggests that UV flux and colour variations observed in both FSRQs and BL Lacs are predominantly driven by synchrotron emission from relativistic jet electrons. Within the one zone leptonic emission model, a BWB trend can arise from the injection of freshly accelerated electrons with a harder energy distribution than the pre-existing cooler electron population (Kirk et al., 1998; Mastichiadis and Kirk, 2002). Notably, the two sources (one FSRQ and one BL Lac) in this study and the five sources reported by Reshma et al. (2024) that showed BWB in UV (that includes one FSRQ and four BL Lacs) are γ -ray loud sources detected by the *Fermi*-LAT (Ackermann et al., 2015), further supporting the dominance of jet emission in these sources.

6. Summary

The UV variability properties of AGN remain relatively less explored compared to other wavelengths. Nevertheless, some studies do exist from HST (Dolan and Clark, 2004), IUE (Edelson et al., 1991; Sukanya et al., 2018) and UVIT (Reshma et al., 2024) observations. In this work, we investigated UV variability on hour timescales using observations obtained with UVIT. Our sample comprises 24 radio-loud (jetted) AGN, that includes 17 BL Lacs, 6 FSRQs and one radio-loud NLSy1 galaxy. The main results of this study are summarized below:

- (i) We detected UV variability in 18 out of the 24 sources, which includes the radio-loud NLSy1 galaxy 1H 0323+342, 5 FSRQs and 12 BL Lacs. All the variable sources are jet dominated systems, strongly suggesting that the observed UV variability is driven by processes occurring within their relativistic jets.
- (ii) We found the amplitude of variability, σ_m in the NUV band to range from 0.010 mag to 0.046 mag, while in the FUV band, we found σ_m to span a wider range between 0.010 mag to 0.247 mag. For the three sources with simultaneous FUV and NUV observations, the variability amplitude in FUV is larger than that in the NUV band for CTA 102 and PKS 0447–439. This suggests that AGN may exhibit stronger variability at shorter UV

wavelengths. However, a larger sample with simultaneous FUV and NUV coverage is required to confirm this trend robustly.

- (iii) Constrained by the simultaneous observations in FUV and NUV bands, we investigated spectral variations in three sources, by generating colour magnitude diagrams. Of the three sources, significant colour variations were detected in two sources, namely, CTA 102 (FSRQ) and PKS 0447–439 (BL Lac). Both sources exhibited a clear BWB trend, which is most plausibly explained by the injection of fresh electrons with an energy distribution harder than the pre-existing cooler electrons in their jet.

The observations reported here on the UV flux and spectral variations in our sample of γ -ray detected blazars favour a jet based origin of their variations. Future UV observations of a large number of blazars, particularly with simultaneous FUV and NUV observations will be crucial to establish whether both FSRQs and BL Lacs show a BWB behaviour in the UV band and if there is any potential connection between UV colour variability and the γ -ray brightness state of these sources.

Acknowledgements

We sincerely thank the referee for the constructive comments and insightful suggestions, which have been invaluable in enhancing the quality and clarity of the manuscript. This research utilizes data from the *AstroSat* mission led by the Indian Space Research Organization with the archival access provided by the Indian Space Science Data Centre (ISSDC). The UVIT data used in this work were processed by the Payload Operation Centre (POC) of the Indian Institute of Astrophysics (IIA), Bengaluru. The UVIT instrument was developed through a collaborative effort involving IIA, the Inter-University Centre for Astronomy and Astrophysics (IUCAA), the Tata Institute of Fundamental Research (TIFR), ISRO and the Canadian Space Agency (CSA). A.K.M. acknowledges the support from the European Research Council (ERC) under the European Union’s Horizon 2020 research and innovation program (grant No. 951549). One of the authors (SBG) thanks the Inter-University Centre for Astronomy and Astrophysics (IUCAA), Pune, India for the Visiting Associateship.

References

- Abdalla, H., Aharonian, F., Ait Benkhali, F., Angüner, E.O., Arakawa, M., Arcaro, C., Armand, C., Arrieta, M., Backes, M., Barnard, M., et al., 2019. The γ -ray discovery and multiwavelength study of the blazar 1es 2322- 409. *Mon. Not. R. Astron. Soc.* 482, 3011–3022. doi:10.1093/mnras/sty2686.
- Abdo, A.A., Ackermann, M., Agudo, I., Ajello, M., Aller, H.D., Aller, M.F., Angelakis, E., Arkharov, A.A., Axelsson, M., Bach, U., et al., 2010a. The spectral energy distribution of fermi bright blazars. *Astrophys. J.* 716, 30. doi:10.1088/0004-637X/716/1/30.

- Abdo, A.A., Ackermann, M., Ajello, M., Allafort, A., Antolini, E., Atwood, W.B., Axelsson, M., Baldini, L., Ballet, J., Barbiellini, G., et al., 2010b. Fermi large area telescope first source catalog. *Astrophys. J. Suppl. Ser.* 188, 405. doi:10.1088/0067-0049/188/2/405.
- Abdo, A.A., Ackermann, M., Ajello, M., Atwood, W.B., Axelsson, M., Baldini, L., Ballet, J., Barbiellini, G., Bastieri, D., Baughman, B.M., et al., 2009a. Bright active galactic nuclei source list from the first three months of the fermi large area telescope all-sky survey. *Astrophys. J.* 700, 597. doi:10.1088/0004-637X/700/1/597.
- Abdo, A.A., Ackermann, M., Ajello, M., Baldini, L., Ballet, J., Barbiellini, G., Bastieri, D., Bechtol, K., Bellazzini, R., Berenji, B., et al., 2009b. Radio-loud narrow-line seyfert 1 as a new class of gamma-ray active galactic nuclei. *Astrophys. J.* 707, L142. doi:10.1088/0004-637X/707/2/L142.
- Abdo, A.A., Ackermann, M., Ajello, M., Baldini, L., Ballet, J., Barbiellini, G., Bastieri, D., Bechtol, K., Bellazzini, R., Berenji, B., et al., 2011. Fermi large area telescope observations of markarian 421: The missing piece of its spectral energy distribution. *Astrophys. J.* 736, 131. doi:10.1088/0004-637X/736/2/131.
- Abdollahi, S., Acero, F., Ackermann, M., Ajello, M., Atwood, W.B., Axelsson, M., Baldini, L., Ballet, J., Barbiellini, G., Bastieri, D., et al., 2020. Fermi large area telescope fourth source catalog. *Astrophys. J. Suppl. Ser.* 247, 33. doi:10.3847/1538-4365/ab6bcb.
- Abe, H., Abe, S., Acciari, V., Agudo, I., Aniello, T., Ansoldi, S., Antonelli, L., Engels, A.A., Arcaro, C., Artero, M., et al., 2024. Multi-year characterisation of the broad-band emission from the intermittent extreme bl lac 1es 2344+ 514. *Astron. Astrophys.* 682, A114. doi:10.1051/0004-6361/202347845.
- Abeysekara, A.U., Archambault, S., Archer, A., Benbow, W., Bird, R., Biteau, J., Buchovecky, M., Buckley, J.H., Bugaev, V., Byrum, K., et al., 2016. Veritas and multiwavelength observations of the bl lacertae object 1es 1741+ 196. *Mon. Not. R. Astron. Soc.* 459, 2550–2557. doi:10.1093/mnras/stw664.
- Acero, F., Aharonian, F., Akhperjanian, A.G., Anton, G., De Almeida, U.B., Bazer-Bachi, A.R., Becherini, Y., Behera, B., Benbow, W., Bernlöhr, K., et al., 2010. Pks 2005-489 at vhe: four years of monitoring with hess and simultaneous multi-wavelength observations. *Astron. Astrophys.* 511, A52. doi:10.1051/0004-6361/200913073.
- Ackermann, M., Ajello, M., Allafort, A., Antolini, E., Barbiellini, G., Bastieri, D., Bellazzini, R., Bissaldi, E., Bonamente, E., Bregeon, J., et al., 2014. Multifrequency studies of the peculiar quasar 4c+ 21.35 during the 2010 flaring activity. *Astrophys. J.* 786, 157. doi:10.1088/0004-637X/786/2/157.
- Ackermann, M., Ajello, M., Atwood, W., Baldini, L., Ballet, J., Barbiellini, G., Bastieri, D., Gonzalez, J.B., Bellazzini, R., Bissaldi, E., et al., 2015. The third catalog of active galactic nuclei detected by the fermi large area telescope. *Astrophys. J.* 810, 14. doi:10.1088/0004-637X/810/1/14.
- Ackermann, M., Ajello, M., Ballet, J., Barbiellini, G., Bastieri, D., Bellazzini, R., Blandford, R., Bloom, E., Bonamente, E., Borgland, A., et al., 2012. Multi-wavelength observations of blazar ao 0235+ 164 in the 2008–2009 flaring state. *Astrophys. J.* 751, 159. doi:10.1088/0004-637X/751/2/159.
- Ackermann, M., Anantua, R., Asano, K., Baldini, L., Barbiellini, G., Bastieri, D., Gonzalez, J.B., Bellazzini, R., Bissaldi, E., Blandford, R., et al., 2016. Minute-timescale > 100 mev γ -ray variability during the giant outburst of quasar 3c 279 observed by fermi-lat in 2015 june. *Astrophys. J. Lett.* 824, L20. doi:10.3847/2041-8205/824/2/L20.
- Agrawal, P., 2017. Astrosat: From inception to realization and launch. *J. Astrophys. Astron.* 38, 27. doi:10.1007/s12036-017-9449-6.
- Aharonian, F., Akhperjanian, A., Bazer-Bachi, A., Behera, B., Beilicke, M., Benbow, W., Berge, D., Bernlöhr, K., Boisson, C., Bolz, O., et al., 2007a. An exceptional very high energy gamma-ray flare of pks 2155–304. *Astrophys. J.* 664, L71. doi:10.1086/520635.
- Aharonian, F., Akhperjanian, A., Bazer-Bachi, A., Beilicke, M., Benbow, W., Berge, D., Bernlöhr, K., Boisson, C., Bolz, O., Borrel, V., et al., 2006. Discovery of very high energy γ -ray emission from the bl lacertae object h 2356-309 with the hess cherenkov telescopes. *Astron. Astrophys.* 455, 461–466. doi:10.1051/0004-6361:20054732.
- Aharonian, F., Akhperjanian, A., De Almeida, U.B., Bazer-Bachi, A., Behera, B., Beilicke, M., Benbow, W., Bernlöhr, K., Boisson, C., Bolz, O., et al., 2007b. New constraints on the mid-ir ebl from the hess discovery of vhe γ -rays from 1es 0229+ 200. *Astron. Astrophys.* 475, L9–L13. doi:10.1051/0004-6361:20078462.
- Aharonian, F., Akhperjanian, A.G., Aye, K.M., Bazer-Bachi, A.R., Beilicke, M., Benbow, W., Berge, D., Berghaus, P., Bernlöhr, K., Boisson, C., et al., 2005. Discovery of vhe gamma rays from pks 2005–489. *Astron. Astrophys.* 436, L17–L20. doi:10.1051/0004-6361:200500113.
- Ahnen, M.L., Ansoldi, S., Antonelli, L.A., Antoranz, P., Arcaro, C., Babic, A., Banerjee, B., Bangale, P., de Almeida, U.B., Barrio, J.A., et al., 2017. Magic detection of very high energy γ -ray emission from the low-luminosity blazar 1es 1741+ 196. *Mon. Not. R. Astron. Soc.* 468, 1534–1541. doi:10.1093/mnras/stx472.
- Ai, Y.L., Yuan, W., Zhou, H.Y., Wang, T.G., Dong, X.B., Wang, J.G., Lu, H.L., 2010. Dependence of the optical/ultraviolet variability on the emission-line properties and eddington ratio in active galactic nuclei. *Astrophys. J. Lett.* 716, L31. doi:10.1088/2041-8205/716/1/L31.

- Akritas, M.G., Bershad, M.A., 1996. Linear regression for astronomical data with measurement errors and intrinsic scatter. arXiv preprint astro-ph/9605002 doi:10.48550/arXiv.astro-ph/9605002.
- Albert, J., Aliu, E., Anderhub, H., Antoranz, P., Armada, A., Asensio, M., Baixeras, C., Barrio, J.A., Bartko, H., Bastieri, D., et al., 2006. Discovery of very high energy γ -rays from markarian 180 triggered by an optical outburst. *Astrophys. J.* 648, L105. doi:10.1086/508020.
- Albert, J., Aliu, E., Anderhub, H., Antoranz, P., Armada, A., Baixeras, C., Barrio, J.A., Bartko, H., Bastieri, D., Becker, J.K., et al., 2007. Variable very high energy γ -ray emission from markarian 501. *Astrophys. J.* 669, 862. doi:10.1086/521382.
- Aleksić, J., Blanch, O., Antonelli, L.A., Bonnoli, G., Antoranz, P., Backes, M., Barrio, J.A., Bastieri, D., Becerra González, J., Berger, K., Bednarek, W., Berdyugin, A., Bernardini, E., Biland, A., Boller, A., Braun, I., Bock, R.K., Borla Tridon, D., Bretz, T., Canellas, A., ..., 2011. MAGIC discovery of very high energy emission from the FSRQ PKS 1222+21. *Astrophys. J. Lett.* 730, L8. doi:10.1088/2041-8205/730/1/L8.
- Aliu, E., Archambault, S., Arlen, T., Aune, T., Barnacka, A., Beilicke, M., Benbow, W., Berger, K., Bird, R., Bouvier, A., et al., 2014. Investigating broadband variability of the tev blazar 1es 1959+ 650. *Astrophys. J.* 797, 89. doi:10.1088/0004-637X/797/2/89.
- Amaya-Almazán, R.A., Chavushyan, V., Patiño-Álvarez, V.M., 2020. Multiwavelength analysis and the difference in the behavior of the spectral features during the 2010 and 2014 flaring periods of the blazar 3c 454.3. *Astrophys. J.* 906, 5. doi:10.3847/1538-4357/abc689.
- Arlen, T., Aune, T., Beilicke, M., Benbow, W., Bouvier, A., Buckley, J.H., Bugaev, V., Cesarini, A., Ciupik, L., Connolly, M.P., et al., 2013. Rapid tev gamma-ray flaring of bl lacertae. *Astrophys. J.* 762, 92. doi:10.1088/0004-637X/762/2/92.
- Bachev, R., Semkov, E., Strigachev, A., Gupta, A.C., Gaur, H., Mihov, B., Boeva, S., Slavcheva-Mihova, L., 2012. The nature of the intra-night optical variability in blazars. *Mon. Not. R. Astron. Soc.* 424, 2625–2634. doi:10.1111/j.1365-2966.2012.21310.x.
- Belloni, T.M., 2010. *The Jet Paradigm* ed T. Belloni. Berlin: Springer.
- Berger, K., 2011. Overview of the results from extra-galactic observations with the magic telescopes. arXiv preprint arXiv:1109.5860.
- Boller, T., Brandt, W.N., Fink, H., 1996. Soft x-ray properties of narrow-line seyfert 1 galaxies. *Astron. Astrophys.*, v. 305, p. 53 305, 53. doi:10.48550/arXiv.astro-ph/9504093.
- Bonning, E., Urry, C.M., Bailyn, C., Buxton, M., Chatterjee, R., Coppi, P., Fossati, G., Isler, J., Maraschi, L., 2012. Smarts optical and infrared monitoring of 12 gamma-ray bright blazars. *Astrophys. J.* 756, 13. doi:10.1088/0004-637X/756/1/13.
- Cai, J.T., Kurtanidze, S.O., Liu, Y., Kurtanidze, O.M., Nikolashvili, M.G., Xiao, H., Fan, J., 2022. Long-term optical monitoring of the tev bl lacertae object 1es 2344+ 514. *Astrophys. J. Suppl. Ser.* 260, 47. doi:10.3847/1538-4365/ac666b.
- Chen, X., Hu, S., Jiang, Y., Xu, J., Huang, S., Zhou, R., Yin, H., Guo, D., Li, Y., Li, H., 2025. Study on the multi-wavelength variation of 3c 454.3. *Sci. Rep.* 15, 8525. doi:10.1038/s41598-025-93386-7.
- Ciprini, S., Cheung, C., 2020. Fermi lat detection of renewed gev gamma-ray flaring activity from oq 334 (b2 1420+ 32). *Astron. Telegram* 13382, 1.
- Costamante, L., Ghisellini, G., Giommi, P., Tagliaferri, G., Celotti, A., Chiaberge, M., Fossati, G., Maraschi, L., Tavecchio, F., Treves, A., et al., 2001. Extreme synchrotron bl lac objects-stretching the blazar sequence. *Astron. Astrophys.* 371, 512–526. doi:10.1051/0004-6361:20010412.
- D’Amicis, R., Nesci, R., Massaro, E., Maesano, M., Montagni, F., D’Alessio, F., 2002. Spectral variability of bl lac objects. *Publ. Astron. Soc. Aust.* 19, 111–113. doi:10.1071/AS01113.
- D’Ammando, F., Angioni, R., Orienti, M., Sitarek, J., Nozaki, S., Lindfors, E., Bonnoli, G., Fallah Ramazani, V., Jorstad, S.G., Acciari, V.A., Ansoldi, S., Antonelli, L.A., Arbet Engels, A., Artero, M., Asano, K., Baack, D., Babic, A., Baquero, A., Barres de Almeida, U., et al., 2021. Multi-wavelength observations in 2019–2020 of a new very-high-energy gamma-ray emitter: the flat spectrum radio quasar qso b1420+326, in: *Proc. 37th Int. Cosmic Ray Conf. (ICRC 2021)*, SISSA. p. 775. doi:10.22323/1.395.0775.
- De La Calle Perez, I., Bond, I.H., Boyle, P.J., Bradbury, S.M., Buckley, J.H., Carter-Lewis, D.A., Celik, O., Cui, W., Dowdall, C., Duke, C., et al., 2003. Search for high-energy gamma rays from an x-ray-selected blazar sample. *Astrophys. J.* 599, 909. doi:10.1086/379544.
- Devanand, P., Gupta, A.C., Jithesh, V., Wiita, P.J., 2022. Study of x-ray intraday variability of hbl blazars based on observations obtained with xmm-newton. *Astrophys. J.* 939, 80. doi:10.3847/1538-4357/ac9064.
- Dolan, J.F., Clark, L.L., 2004. A search for short-timescale microvariability in active galactic nuclei in the ultraviolet. *Astrophys. J.* 607, 84. doi:10.1086/383460.
- Dominici, T.P., Abraham, Z., Teixeira, R., Benevides-Soares, P., 2004. Long-term optical variability of the blazars pks 2005- 489 and pks 2155- 304. *Astron. J.* 128, 47. doi:10.1086/421361.

- Donato, D., 2010. Fermi LAT observed another strong GeV flare from 4C 21.35 (PKS 1222+21). *Astron. Telegram* 2584, 1.
- D'Ammando, F., 2019. Relativistic jets in gamma-ray-emitting narrow-line seyfert 1 galaxies. *Galaxies* 7, 87. doi:10.3390/galaxies7040087.
- D'Ammando, F., 2020a. Gamma-ray-emitting narrow-line seyfert 1 galaxies: the swift view. *Mon. Not. R. Astron. Soc.* 496, 2213–2229. doi:10.1093/mnras/staa1580.
- D'Ammando, F., 2020b. Short time-scale variability of γ -ray-emitting narrow-line seyfert 1 galaxies in optical and uv bands. *Mon. Not. R. Astron. Soc.* 498, 859–874. doi:10.1093/mnras/staa2471.
- D'Ammando, F., Raiteri, C.M., Villata, M., Acosta-Pulido, J.A., Agudo, I., Arkharov, A.A., Bachev, R., Baida, G.V., Benítez, E., Borman, G.A., et al., 2019. Investigating the multiwavelength behaviour of the flat spectrum radio quasar cta 102 during 2013–2017. *Mon. Not. R. Astron. Soc.* 490, 5300–5316. doi:10.1093/mnras/stz2792.
- Edelson, R.A., Saken, J., Pike, G., Urry, C.M., George, I.M., Warwick, R.S., Miller, H.R., Carini, M.T., Webb, J.R., 1991. Rapid ultraviolet variability in the bl lacertae object pks 2155-304. *Astrophys. J., Part 2-Letters (ISSN 0004-637X)*, vol. 372, May 1, 1991, p. L9-L12. SERC-supported research. 372, L9–L12. doi:10.1086/186011.
- Elvis, M., Plummer, D., Schachter, J., Fabbiano, G., 1992. The einstein slew survey. *Astrophys. J. Suppl. Ser. (ISSN 0067-0049)*, vol. 80, no. 1, May 1992, p. 257-303. 80, 257–303.
- Falomo, R., 1991. On the galaxy surrounding the bl lac object h2356-309. *Astron. J. (ISSN 0004-6256)*, vol. 101, March 1991, p. 821-824. 101, 821–824.
- Falomo, R., Maraschi, L., Tanzi, E., Treves, A., 1987. The redshift of the bl lacertae object pks 2005-489. *Astrophys. J., Part 2-Letters to the Editor (ISSN 0004-637X)*, vol. 318, July 15, 1987, p. L39-L41. 318, L39–L41.
- Farina, E.P., Decarli, R., Falomo, R., Treves, A., Raiteri, C.M., 2012. The optical spectrum of pks 1222+ 216 and its black hole mass. *Mon. Not. R. Astron. Soc.* 424, 393–398. doi:10.1111/j.1365-2966.2012.21209.x.
- Feigelson, E., Bradt, H., McClintock, J., Remillard, R., Urry, C., Tapia, S., Geldzahler, B., Johnston, K., Romanishin, W., Wehinger, P., et al., 1986. H 0323+ 022-a new bl lacertae object with extremely rapid variability. *Astrophys. J., Part 1 (ISSN 0004-637X)*, vol. 302, March 1, 1986, p. 337-351. 302, 337–351. doi:10.1086/163993.
- Fiorucci, M., Ciprini, S., Tosti, G., 2004. The continuum spectral features of blazars in the optical region. *Astron. Astrophys.* 419, 25–34. doi:10.1051/0004-6361:20034218.
- Forman, W., Jones, C., Cominsky, L., Julien, P., Murray, S., Peters, G., Tananbaum, H., Giacconi, R., 1978. The fourth uhuru catalog of x-ray sources. *Astrophys. J., Suppl. Ser.*, Vol. 38, p. 357-412 38, 357–412.
- Foschini, L., 2020. Jetted narrow-line seyfert 1 galaxies & co.: Where do we stand? *Universe* 6, 136. doi:10.3390/universe6090136.
- Furniss, A., Fumagalli, M., Falcone, A., Williams, D.A., 2013. The blazar emission environment: Insight from soft x-ray absorption. *Astrophys. J.* 770, 109. doi:10.1088/0004-637X/770/2/109.
- Gaur, H., Gupta, A.C., Bachev, R., Strigachev, A., Semkov, E., Wiita, P., Kurtanidze, O., Darriba, A., Damljanovic, G., Chanishvili, R., et al., 2019. Optical variability of tev blazars on long time-scales. *Mon. Not. R. Astron. Soc.* 484, 5633–5644. doi:10.1093/mnras/stz322.
- Gaur, H., Gupta, A.C., Strigachev, A., Bachev, R., Semkov, E., Wiita, P.J., Peneva, S., Boeva, S., Kacharov, N., Mihov, B., et al., 2012. Quasi-simultaneous two-band optical variability of the blazars 1es 1959+ 650 and 1es 2344+ 514. *Mon. Not. R. Astron. Soc.* 420, 3147–3162. doi:10.1111/j.1365-2966.2011.20243.x.
- Ghisellini, G., Ceca, R.D., Volonteri, M., Ghirlanda, G., Tavecchio, F., Foschini, L., Tagliaferri, G., Haardt, F., Pareschi, G., Grindlay, J., 2010a. Chasing the heaviest black holes of jetted active galactic nuclei. *Mon. Not. R. Astron. Soc.* 405, 387–400. doi:10.1111/j.1365-2966.2010.16449.x.
- Ghisellini, G., Tavecchio, F., Foschini, L., Ghirlanda, G., 2011. The transition between bl lac objects and flat spectrum radio quasars. *Mon. Not. R. Astron. Soc.* 414, 2674–2689. doi:10.1111/j.1365-2966.2011.18578.x.
- Ghisellini, G., Tavecchio, F., Foschini, L., Ghirlanda, G., Maraschi, L., Celotti, A., 2010b. General physical properties of bright fermi blazars. *Mon. Not. R. Astron. Soc.* 402, 497–518. doi:10.1111/j.1365-2966.2009.15898.x.
- Gliozzi, M., Sambruna, R., Jung, I., Krawczynski, H., Horan, D., Tavecchio, F., 2006. Long-term x-ray and tev variability of mrk 501. *Astrophys. J.* 646, 61–75. doi:10.1086/504700.
- Goswami, P., Zacharias, M., Zech, A., Chandra, S., Boettcher, M., Sushch, I., 2024. The variety of extreme blazars in the astrosat view. *Astron. Astrophys.* 682, A134. doi:10.1051/0004-6361/202348121.
- Gregory, P.C., Vavasour, J.D., Scott, W.K., Condon, J.J., 1994. The parkes-mit-nrao (pmn) map catalog of radio sources covering-88 deg less than delta less than-37 deg at 4.85 ghz. *Astrophys. J. Suppl. Ser.*, vol. 90, no. 1, p. 173-177 90, 173–177.

- Grupe, D., Mathur, S., 2004. Mbh- σ relation for a complete sample of soft x-ray-selected active galactic nuclei. *Astrophys. J.* 606, L41. doi:10.1086/420975.
- Gupta, A.C., Kushwaha, P., Carrasco, L., Xu, H., Wiita, P.J., Escobedo, G., Porras, A., Recillas, E., Mayya, Y.D., Chavushyan, V., Villarroel, B., Zhang, Z., 2022. Long-term Multiband Near-infrared Variability of the Blazar OJ 287 during 2007-2021. *Astrophys. J.* 260, 39. doi:10.3847/1538-4365/ac6c2c, arXiv:2205.03618.
- Hartman, R.C., Bertsch, D.L., Bloom, S.D., Chen, A.W., Deines-Jones, P., Esposito, J.A., Fichtel, C.E., Friedlander, D.P., Hunter, S.D., McDonald, L.M., et al., 1999. The third egret catalog of high-energy gamma-ray sources. *Astrophys. J. Suppl. Ser.* 123, 79.
- Heidt, J., Nilsson, K., Fried, J., Takalo, L., Sillanpää, A., 1999. Ies 1741+ 196: a bl lacertae object in a triplet of interacting galaxies? arXiv preprint astro-ph/9906129 doi:10.48550/arXiv.astro-ph/9906129.
- Holder, J., Bond, I., Boyle, P., Bradbury, S., Buckley, J., Carter-Lewis, D., Cui, W., Dowdall, C., Duke, C., De La Calle Perez, I., et al., 2002. Detection of tev gamma rays from the bl lacertae object Ies 1959+ 650 with the whipple 10 meter telescope. *Astrophys. J.* 583, L9. doi:10.1086/367816.
- Hutter, D.J., Mufson, S.L., 1981. An optical and x-ray survey of s-type markarian galaxies. *Astron. J.*, vol. 86, Nov. 1981, p. 1585-1594. 86, 1585–1594.
- Impey, C.D., Tapia, S., 1990. The optical polarization properties of quasars. *Astrophys. J.*, Part 1 (ISSN 0004-637X), vol. 354, May 1, 1990, p. 124-139. Research supported by the Space Telescope Science Institute. 354, 124–139.
- Jones, D.H., Read, M.A., Saunders, W., Colless, M., Jarrett, T., Parker, Q.A., Fairall, A.P., Mauch, T., Sadler, E.M., Watson, F.G., et al., 2009. The 6df galaxy survey: final redshift release (dr3) and southern large-scale structures. *Mon. Not. R. Astron. Soc.* 399, 683–698. doi:10.1111/j.1365-2966.2009.15338.x.
- Jorstad, S.G., Marscher, A.P., Smith, P.S., Larionov, V.M., Agudo, I., Gurwell, M., Wehrle, A.E., Lähteenmäki, A., Nikolashvili, M.G., Schmidt, G.D., et al., 2013. A tight connection between gamma-ray outbursts and parsec-scale jet activity in the quasar 3c 454.3. *Astrophys. J.* 773, 147. doi:10.1088/0004-637X/773/2/147.
- Joseph, P., Stalin, C.S., Tandon, S.N., Ghosh, S.K., 2021. Curvit: An open-source python package to generate light curves from uvit data. *J. Astrophys. Astron.* 42, 25. doi:10.1007/s12036-020-09680-5.
- Joseph, P., TANDON, S.N., GHOSH, S.K., STALIN, C.S., 2025. Uvit data release version 7: Regenerated high-level uvit data products: P. joseph et al. *J. Astrophys. Astron.* 46, 41. doi:10.1007/s12036-025-10069-5.
- Kalita, N., Gupta, A.C., Gu, M., 2021. Optical variability of a newly discovered blazar sample from the bzcata catalog. *Astrophys. J. Suppl. Ser.* 257, 41. doi:10.3847/1538-4365/ac1e9c.
- Kapanadze, B., Gurchumelia, A., Aller, M., 2023. Long-term x-ray outburst in the tev-detected blazar mrk 501 in 2021–2022: Further clues for the emission and unstable processes. *Astrophys. J. Suppl. Ser.* 268, 20. doi:10.3847/1538-4365/ace69f.
- Kellermann, K.I., Sramek, R., Schmidt, M., Shaffer, D.B., Green, R., 1989. VLA observations of objects in the palomar bright quasar survey. *Astron. J.* (ISSN 0004-6256), vol. 98, Oct. 1989, p. 1195-1207. 98, 1195–1207.
- Kelly, B.C., 2007. Some aspects of measurement error in linear regression of astronomical data. *Astrophys. J.* 665, 1489. doi:10.1086/519947.
- Kirk, J., Rieger, F., Mastichiadis, A., 1998. Particle acceleration and synchrotron emission in blazar jets. arXiv preprint astro-ph/9801265 333, 452–458. doi:10.48550/arXiv.astro-ph/9801265.
- Kishore, S., Gupta, A.C., Wiita, P.J., 2024. Rapid Optical Flares in the Blazar OJ 287 on Intraday Timescales with TESS. *Astrophys. J.* 960, 11. doi:10.3847/1538-4357/ad0b80, arXiv:2311.02368.
- Kishore, S., Gupta, A.C., Wiita, P.J., Tiwari, S., 2024. Rapid optical flare in the extreme teraelectronvolt blazar Ies 0229+ 200 on intraday timescales with the transiting exoplanet survey satellite. *Astron. Astrophys.* 690, A223. doi:10.1051/0004-6361/202449888.
- Komossa, S., Voges, W., Xu, D., Mathur, S., Adorf, H.M., Lemson, G., Duschl, W.J., Grupe, D., 2006. Radio-loud narrow-line type 1 quasars. *Astron. J.* 132, 531. doi:10.1086/505043.
- Krawczynski, H., Hughes, S.B., Horan, D., Aharonian, F., Aller, M.F., Aller, H., Boltwood, P., Buckley, J., Coppi, P., Fossati, G., et al., 2004. Multiwavelength observations of strong flares from the tev blazar Ies 1959+ 650. *Astrophys. J.* 601, 151. doi:10.1086/380393.
- Kuznetsov, S., 2024. Black hole mass estimate in oj 287 based on the bulk-motion comptonization model. *Mon. Not. R. Astron. Soc.* 535, 3732–3737.
- Lampton, M., Lieu, R., Schmitt, J., Bowyer, S., Voges, W., Lewis, J., Wu, X., 1997. An all-sky catalog of faint extreme ultraviolet sources. *Astrophys. J. Suppl. Ser.* 108, 545.
- Large, M.I., Mills, B.Y., Little, A.G., Crawford, D.F., Sutton, J.M., 1981. The molonglo reference catalogue of radio sources. *Mon. Not. R. Astron. Soc.* 194, 693–704.

- Leighly, K.M., 1999a. A comprehensive spectral and variability study of narrow-line seyfert 1 galaxies observed by asca. ii. spectral analysis and correlations. *Astrophys. J. Suppl. Ser.* 125, 317. doi:10.1086/313287.
- Leighly, K.M., 1999b. A comprehensive spectral and variability study of narrow-line seyfert 1 galaxies observed by asca. i. observations and time series analysis. *Astrophys. J. Suppl. Ser.* 125, 297. doi:10.1086/313277.
- Li, H.Z., Guo, D.F., Qin, L.H., Yi, T.F., Liu, F., Gao, Q.G., Chang, X., 2024. The optical intra-day variability of bl lacertae object 2200+ 420. *Mon. Not. R. Astron. Soc.* 528, 6823–6835. doi:10.1093/mnras/stae422.
- Liu, F., Zhao, G., Wu, X.B., 2006. Harmonic qpos and thick accretion disk oscillations in the bl lacertae object ao 0235+164. *Astrophys. J.* 650, 749.
- Lynden-Bell, D., 1969. Galactic nuclei as collapsed old quasars. *Nature* 223, 690–694. doi:10.1038/223690a0.
- Malizia, A., Bassani, L., Dean, A.J., McCollough, M., Stephen, J.B., Zhang, S.N., Paciesas, W.S., 2000. Hard x-ray detection of the high-redshift quasar 4c71. 07. *Astrophys. J.* 531, 642. doi:10.1086/308521.
- Manzoor, A., Shah, Z., Sahayanathan, S., Iqbal, N., Dar, A.A., 2024. Broad-band spectral and temporal study of ton 599 during the brightest 2023 january flare. *Mon. Not. R. Astron. Soc.* 529, 1356–1364. doi:10.1093/mnras/stae588.
- Marscher, A.P., Gear, W.K., 1985. Models for high-frequency radio outbursts in extragalactic sources, with application to the early 1983 millimeter-to-infrared flare of 3c 273. *Astrophys. J., Part 1 (ISSN 0004-637X)*, vol. 298, Nov. 1, 1985, p. 114–127. 298, 114–127. doi:10.1086/163592.
- Masetti, N., Bassani, L., Bazzano, A., Bird, A.J., Dean, A.J., Malizia, A., Norci, L., Palazzi, E., Schwöpe, A.D., Stephen, J.B., et al., 2006. Unveiling the nature of integral objects through optical spectroscopy-iv. a study of six new hard x-ray sources. *Astron. Astrophys.* 455, 11–19. doi:10.1051/0004-6361:20065111.
- Mastichiadis, A., Kirk, J.G., 2002. Models of variability in blazar jets. *Publ. Astron. Soc. Aust.* 19, 138–142. doi:10.1071/AS01108.
- Maurya, S., Majumdar, J., Sahu, N., Prince, R., et al., 2025. On the origin of multifrequency temporal and spectral variability in ton 599. *Publ. Astron. Soc. Aust.* 42, e053.
- Meng, N., Zhang, X., Wu, J., Ma, J., Zhou, X., 2018. Multi-color optical monitoring of 10 blazars from 2005 to 2011. *Astrophys. J. Suppl. Ser.* 237, 30. doi:10.3847/1538-4365/aacffe.
- Mirzoyan, R., 2017. Detection of very-high-energy gamma-ray emission from the fsrq ton 0599 with the magic telescopes. *Astron. Telegram* 11061, 1.
- Mishra, H.D., Dai, X., Chen, P., Cheng, J., Jayasinghe, T., Tucker, M.A., Vallety, P.J., Bersier, D., Bose, S., Do, A., et al., 2021. The changing-look blazar b2 1420+ 32. *Astrophys. J.* 913, 146. doi:10.3847/1538-4357/abf63.
- Mondal, S.K., Das, S., Gupta, N., 2023. Exploring the emission mechanisms of mrk 180 with long-term x-ray and γ -ray data. *Astrophys. J.* 948, 75. doi:10.3847/1538-4357/acc46b.
- Moore, R.L., Stockman, H.S., 1981. The class of highly polarized quasars-observations and description. *Astrophys. J., Part 1*, vol. 243, Jan. 1, 1981, p. 60–75. 243, 60–75. doi:10.1086/158567.
- Muriel, H., Donzelli, C., Rovero, A.C., Pichel, A., 2015. The bl-lac gamma-ray blazar pks 0447-439 as a probable member of a group of galaxies at $z = 0.343$. *Astron. Astrophys.* 574, A101. doi:10.1051/0004-6361/201425050.
- Negi, V., Joshi, R., Chand, K., Chand, H., Wiita, P., Ho, L.C., Singh, R.S., 2022. Optical flux and colour variability of blazars in the ztf survey. *Mon. Not. R. Astron. Soc.* 510, 1791–1800. doi:10.1093/mnras/stab3591.
- Nieppola, E., Tornikoski, M., Valtaoja, E., 2006. Spectral energy distributions of a large sample of bl lacertae objects. *Astron. Astrophys.* 445, 441–450. doi:10.1051/0004-6361:20053316.
- Nilsson, K., Lindfors, E., Takalo, L., Reinthal, R., Berdyugin, A., Sillanpää, A., Ciprini, S., Halkola, A., Heinämäki, P., Hovatta, T., et al., 2018. Long-term optical monitoring of tev emitting blazars-i. data analysis. *Astron. Astrophys.* 620, A185. doi:10.1051/0004-6361/201833621.
- Nishiyama, T., 1999. Detection of a new tev gamma-ray source of bl lac object 1es 1959+ 650, in: *Proc. 26th Int. Cosmic Ray Conf. August 17-25, 1999. Salt Lake City, Utah, USA. Under the auspices of the International Union of Pure and Applied Physics (IUPAP). Volume 3. Edited by D. Kieda, M. Salamon, and B. Dingus, p. 370, p. 370.*
- O'Brien, S., 2017. VERITAS detection of VHE emission from the optically bright quasar OJ 287. *arXiv e-prints*, arXiv:1708.02160doi:10.48550/arXiv.1708.02160, arXiv:1708.02160.
- Ojha, V., Krishna, G., Chand, H., 2019. Intra-night optical monitoring of three γ -ray detected narrow-line seyfert 1 galaxies. *Mon. Not. R. Astron. Soc.* 483, 3036–3047. doi:10.1093/mnras/sty3288.
- Orienti, M., D'Ammando, F., Giroletti, M., Dallacasa, D., Giovannini, G., Ciprini, S., 2020. Radio vlba polarization and multiband monitoring of the high-redshift quasar s5 0836+710 during a high-activity period. *Mon. Not. R. Astron. Soc.* 491, 858–873. doi:10.1093/mnras/stz2949.
- Osterbrock, D.E., Pogge, R.W., 1985. The spectra of narrow-line seyfert 1 galaxies. *Astrophys. J., Part 1 (ISSN 0004-637X)*, vol. 297, Oct. 1, 1985, p. 166–176. 297, 166–176.

- Padovani, P., Alexander, D., Assef, R., De Marco, B., Giommi, P., Hickox, R., Richards, G., Smolčić, V., Hatziminaoglou, E., Mainieri, V., et al., 2017. Active galactic nuclei: what's in a name? *Astron. Astrophys. Rev.* 25, 2. doi:10.1007/s00159-017-0102-9.
- Paliya, V.S., Ajello, M., Rakshit, S., Mandal, A.K., Stalin, C.S., Kaur, A., Hartmann, D., 2018. Gamma-ray-emitting narrow-line seyfert 1 galaxies in the sloan digital sky survey. *Astrophys. J. Lett.* 853, L2. doi:10.3847/2041-8213/aaa5ab.
- Paliya, V.S., Marcutulli, L., Ajello, M., Joshi, M., Sahayanathan, S., Rao, A., Hartmann, D., 2017. General physical properties of cgrabs blazars. *Astrophys. J.* 851, 33. doi:10.3847/1538-4357/aa98e1.
- Paliya, V.S., Parker, M., Fabian, A., Stalin, C., 2016. Broad-band observations of high redshift blazars. *Astrophys. J.* 825, 74. doi:10.3847/0004-637X/825/1/74.
- Paliya, V.S., Sahayanathan, S., Parker, M.L., Fabian, A.C., Stalin, C.S., Anjum, A., Pandey, S.B., 2014. The peculiar radio-loud narrow line seyfert 1 galaxy 1h 0323+ 342. *Astrophys. J.* 789, 143. doi:10.1088/0004-637X/789/2/143.
- Paliya, V.S., Sahayanathan, S., Stalin, C., 2015. Multi-wavelength observations of 3c 279 during the extremely bright gamma-ray flare in 2014 march–april. *Astrophys. J.* 803, 15. doi:10.1088/0004-637X/803/1/15.
- Paliya, V.S., Stalin, C.S., Kumar, B., Kumar, B., Bhatt, V.K., Pandey, S.B., Yadav, R.K.S., 2013. Intranight optical variability of γ -ray-loud narrow-line seyfert 1 galaxies. *Mon. Not. R. Astron. Soc.* 428, 2450–2458. doi:10.1093/mnras/sts217.
- Paltani, S., Courvoisier, T.J., 1994. Systematic study of the ultraviolet variability of active galactic nuclei. Technical Report. SCAN-9410336.
- Pan, H.W., Yuan, W., Yao, S., Komossa, S., Jin, C., 2018. Independent estimation of black hole mass for the γ -ray-detected archetypal narrow-line seyfert 1 galaxy 1h 0323+ 342 from x-ray variability. *Astrophys. J.* 866, 69.
- Pandey, A., Gupta, A.C., Wiita, P.J., 2017. X-ray intraday variability of five tev blazars with nustar. *Astrophys. J.* 841, 123. doi:10.3847/1538-4357/aa705e.
- Pandey, A., Gupta, A.C., Wiita, P.J., 2018. X-ray flux and spectral variability of six tev blazars with nustar. *Astrophys. J.* 859, 49. doi:10.3847/1538-4357/aabc5b.
- Pandey, A., Stalin, C.S., 2022. Detection of minute-timescale γ -ray variability in bl lacertae by fermi-lat. *Astron. Astrophys.* 668, A152. doi:10.1051/0004-6361/202244648.
- Papadakis, I., Villata, M., Raiteri, C., 2007. The long-term optical spectral variability of bl lacertae. *Astron. Astrophys.* 470, 857–863. doi:10.1051/0004-6361:20077516.
- Patel, S.R., Chitnis, V.R., Shukla, A., Rao, A.R., Nagare, B.J., 2018. Temporal variability and estimation of jet parameters for ton 599. *Astrophys. J.* 866, 102. doi:10.3847/1538-4357/aae1fc.
- Perlman, E.S., Madejski, G., Stocke, J.T., Rector, T.A., 1999. X-ray spectral variability of pks 2005–489 during the spectacular 1998 november flare. *Astrophys. J.* 523, L11.
- Perlman, E.S., Padovani, P., Giommi, P., Sambruna, R., Jones, L.R., Tzioumis, A., Reynolds, J., 1998. The deep x-ray radio blazar survey. i. methods and first results. *Astron. J.* 115, 1253. doi:10.1086/300283.
- Perlman, E.S., Stocke, J.T., Schachter, J.F., Elvis, M., Ellingson, E., Urry, C.M., Potter, M., Impey, C.D., Kolchinsky, P., 1996. The einstein slew survey sample of bl lacertae objects. *Astrophys. J. Suppl. Ser.* v. 104, p. 251 104, 251. doi:10.1086/192300.
- Peterson, B.M., McHardy, I.M., Wilkes, B.J., Berlind, P., Bertram, R., Calkins, M., Collier, S., Huchra, J.P., Mathur, S., Papadakis, I., et al., 2000. X-ray and optical variability in ngc 4051 and the nature of narrow-line seyfert 1 galaxies. *Astrophys. J.* 542, 161. doi:10.1086/309518.
- Prince, R., 2019. Multi-frequency variability study of ton 599 during the high activity of 2017. *Astrophys. J.* 871, 101. doi:10.3847/1538-4357/aaf475.
- Prince, R., Khatoon, R., Stalin, C., 2021a. Broad-band study of oq 334 during its flaring state. *Mon. Not. R. Astron. Soc.* 502, 5245–5258.
- Prince, R., Raman, G., Khatoon, R., Agarwal, A., Gupta, N., Czerny, B., Majumdar, P., 2021b. A comprehensive study of the 2019–2020 flare of oj 287 using astrosat, swift and nustar. *Mon. Not. R. Astron. Soc.* 508, 315–325. doi:10.1093/mnras/stab2545.
- Raiteri, C., Villata, M., Aller, H., Aller, M., Heidt, J., Kurtanidze, O., Lanteri, L., Maesano, M., Massaro, E., Montagnani, F., et al., 2001. Optical and radio variability of the bl lacertae object ao 0235+ 16: A possible 5-6 year periodicity. *Astron. Astrophys.* 377, 396–412. doi:10.1051/0004-6361:20011112.
- Raiteri, C., Villata, M., Larionov, V., Aller, M., Bach, U., Gurwell, M., Kurtanidze, O., Lähteenmäki, A., Nilsson, K., Volvach, A., et al., 2008a. Radio-to-uv monitoring of ao 0235+ 164 by the webt and swift during the 2006–2007 outburst. *Astron. Astrophys.* 480, 339–347. doi:10.1051/0004-6361:20079044.
- Raiteri, C.M., 2025. The variability of blazars throughout the electromagnetic spectrum. *Astron. Astrophys. Rev.* 33, 8. doi:10.1007/s00159-025-00165-4.
- Raiteri, C.M., Villata, M., Carnerero, M.I., Acosta-Pulido, J.A., Larionov, V.M., D'Ammando, F., Arévalo, M.J., Arkharov,

- A.A., Bueno Bueno, A., Di Paola, A., et al., 2014. Infrared properties of blazars: putting the gasp-webt sources into context. *Mon. Not. R. Astron. Soc.* 442, 629–646. doi:10.1093/mnras/stu886.
- Raiteri, C.M., Villata, M., Carnerero, M.I., Acosta-Pulido, J.A., Mirzaqulov, D.O., Larionov, V.M., Romano, P., Vercellone, S., Agudo, I., Arkharov, A.A., et al., 2019. The beamed jet and quasar core of the distant blazar 4c 71.07. *Mon. Not. R. Astron. Soc.* 489, 1837–1849. doi:10.1093/mnras/stz2264.
- Raiteri, C.M., Villata, M., Larionov, V.M., Gurwell, M.A., Chen, W.P., Kurtanidze, O.M., Aller, M.F., Böttcher, M., Calciolone, P., Hroch, F., et al., 2008b. A new activity phase of the blazar 3c 454.3-multifrequency observations by the webt and xmm-newton in 2007–2008. *Astron. Astrophys.* 491, 755–766. doi:10.1051/0004-6361:200810869.
- Rajput, B., Mandal, A.K., Pandey, A., Stalin, C.S., Max-Moerbeck, W., Mathew, B., 2024. Investigation of the correlation between optical and γ -ray flux variations in the blazar ton 599. *Mon. Not. R. Astron. Soc.* 527, 11900–11914. doi:10.1093/mnras/stad4003.
- Rajput, B., Shah, Z., Stalin, C.S., Sahayanathan, S., Rakshit, S., 2021. Correlation between optical and γ -ray flux variations in BL Lacs. *Mon. Not. R. Astron. Soc.* 504, 1772–1786. doi:10.1093/mnras/stab970, arXiv:2104.00402.
- Rajput, B., Stalin, C., Sahayanathan, S., Rakshit, S., Mandal, A.K., 2019. Temporal correlation between the optical and γ -ray flux variations in the blazar 3c 454.3. *Mon. Not. R. Astron. Soc.* 486, 1781–1795. doi:10.1093/mnras/stz941.
- Rakshit, S., Stalin, C.S., Chand, H., Zhang, X.G., 2017. A catalog of narrow line seyfert 1 galaxies from the sloan digital sky survey data release 12. *Astrophys. J. Suppl. Ser.* 229, 39. doi:10.3847/1538-4365/aa6971.
- Rakshit, S., Stalin, C.S., Hota, A., Konar, C., 2018. Rare finding of a 100 kpc large, double-lobed radio galaxy hosted in the narrow-line seyfert 1 galaxy sdss j103024.95+ 551622.7. *Astrophys. J.* 869, 173. doi:10.3847/1538-4357/aafef8.
- Rees, M.J., 1984. Black hole models for active galactic nuclei. IN: *Annu. Rev. Astron. Astrophys.* Volume 22. Palo Alto, CA, Annual Reviews, Inc., 1984, p. 471–506. 22, 471–506.
- Ren, S.S., Zhou, R.X., Zheng, Y.G., Kang, S.J., 2024. The oscillation in evolution of changing-look blazar oq 334. *Astrophys. J.* 976, 124. doi:10.3847/1538-4357/ad83ce.
- Reshma, M., Agarwal, A., Stalin, C.S., Joseph, P.P., Dagore, A., Mandal, A.K., Devaraj, A., Gudennavar, S.B., 2024. Ultraviolet flux and spectral variability study of blazars observed with uvit/astrosat. *Astrophys. J.* 975, 6. doi:10.3847/1538-4357/ad702e.
- Romero, G., Fan, J.H., Nuza, S.E., 2003. The binary black hole scenario for the bl lacertae object ao 0235+ 16. *Chin. J. Astron. Astrophys.* 3, 513–525. doi:10.1088/1009-9271/3/6/513.
- Romero, G.E., Cellone, S.A., Combi, J.A., 2000. Extreme intranight variability in the BL Lacertae object AO 0235+164. *Astron. Astrophys.* 360, L47–L50. doi:10.48550/arXiv.astro-ph/0007407, arXiv:astro-ph/0007407.
- Roy, A., Gupta, A.C., Chitnis, V.R., Cellone, S.A., Raiteri, C.M., Romero, G.E., Wiita, P.J., Chatterjee, A., Combi, J.A., Liao, M., et al., 2023. Study of variability in long-term multiwavelength optical lightcurves of blazar ao 0235+ 164. *Astrophys. J. Suppl. Ser.* 265, 14. doi:10.3847/1538-4365/acb059.
- Sahakyan, N., 2020. Investigation of the γ -ray spectrum of cta 102 during the exceptional flaring state in 2016–2017. *Astron. Astrophys.* 635, A25.
- Sahakyan, N., 2021. Modelling the broad-band emission of 3c 454.3. *Mon. Not. R. Astron. Soc.* 504, 5074–5086. doi:10.1093/mnras/stab1135.
- Sarkar, A., Chitnis, V., Gupta, A., Gaur, H., Patel, S., Wiita, P., Volvach, A., Tornikoski, M., Chamani, W., Enestam, S., et al., 2019. Long-term variability and correlation study of the blazar 3c 454.3 in the radio, nir, and optical wavebands. *Astrophys. J.* 887, 185. doi:10.3847/1538-4357/ab5281.
- Schachter, J.F., Stocke, J.T., Perlman, E., Elvis, M., Remillard, R., Granados, A., Luu, J., Huchra, J.P., Humphreys, R., Urry, C.M., et al., 1993. Ten new bl lacertae objects discovered by an efficient x-ray/radio/optical technique. *Astrophys. J., Part 1 (ISSN 0004-637X)*, vol. 412, no. 2, p. 541–549. 412, 541–549.
- Schmidt, M., 1965. Large redshifts of five quasi-stellar sources. *Astrophys. J.*, vol. 141, p. 1295–141, 1295. doi:10.1086/148217.
- Schwartz, D., Brissenden, R.J.V., Thuoy, I.R., 1989. in: Maraschi, L., Maccacaro, T., Ulrich, M.H. (Eds.), *Lect. Notes Phys.*, Springer. p. 211.
- Shukla, A., Mannheim, K., 2020. Gamma-ray flares from relativistic magnetic reconnection in the jet of the quasar 3c 279. *Nat. Commun.* 11, 4176. doi:10.1038/s41467-020-17912-z.
- Shukla, A., Mannheim, K., Patel, S.R., Roy, J., Chitnis, V.R., Dorner, D., Rao, A.R., Anupama, G.C., Wendel, C., 2018. Short-timescale γ -ray variability in cta 102. *Astrophys. J. Lett.* 854, L26. doi:10.3847/2041-8213/aaacca.
- Sillanpaa, A., Haarala, S., Valtonen, M., Sundelius, B., Byrd, G., 1988. Oj 287-binary pair of supermassive black holes. *Astrophys. J., Part 1 (ISSN 0004-637X)*, vol. 325, Feb. 15, 1988, p. 628–634. Research supported by Nordisk Institut for Teoretisk Atomfysik and NSF. 325, 628–634.

- Sukanya, N., Stalin, C.S., Joseph, P., Rakshit, S., Praveen, D., Damle, R., 2018. Long-term ultraviolet variability of seyfert galaxies. *J. Astrophys. Astron.* 39, 1–13. doi:10.1007/s12036-018-9556-z.
- Tagliaferri, G., Ghisellini, G., Perri, M., Hayashida, M., Balokovic, M., Covino, S., Giommi, P., Madejski, G., Puccetti, S., Sbarrato, T., et al., 2015. Nustar and multifrequency study of the two high-redshift blazars s5 0836+ 710 and pks 2149–306. *Astrophys. J.* 807, 167.
- Tandon, S.N., Postma, J., Joseph, P., Devaraj, A., Subramaniam, A., Barve, I.V., George, K., Ghosh, S.K., Girish, V., Hutchings, J.B., et al., 2020. Additional calibration of the ultraviolet imaging telescope on board astrosat. *Astron. J.* 159, 158. doi:10.3847/1538-3881/ab72a3.
- Tantry, J., Shah, Z., Misra, R., Iqbal, N., Akbar, S., 2024. Probing broadband spectral energy distribution and variability of mrk 501 in the low flux state. *J. High Energy Astrophys.* 44, 393–409. doi:10.1016/j.jheap.2024.10.014.
- Thomas, H.C., Beuermann, K., Reinsch, K., Schwobe, A., Truemper, J., Voges, W., 1998. Identification of soft high galactic latitude rass x-ray sources. i. a complete count-rate limited sample. *Astron. Astrophys.*, v. 335, p. 467–478 (1998) 335, 467–478.
- Tripathi, A., Wiita, P.J., Smith, K.L., 2026. Probable quasi-periodic oscillations in the tess observations of blazars in the swift x-ray survey. *Mon. Not. R. Astron. Soc.* 545, staf2211. doi:10.1093/mnras/staf2211.
- Turner, C.S., Miller, H.R., Maune, J.D., Eggen, J.R., 2022. Optical variability of the very radio-loud narrow line seyfert 1 galaxy, 1h 0323+ 342. *Mon. Not. R. Astron. Soc.* 517, 3257–3262. doi:10.1093/mnras/stac2805.
- Ulrich, M.H., Maraschi, L., Urry, C.M., 1997. Variability of active galactic nuclei. *Annu. Rev. Astron. Astrophys.* 35, 445–502.
- Umayal, S., Paliya, V.S., Saikia, D.J., Stalin, C.S., Muneer, S., Gopinathan, M., 2025. Identification of large-scale (> 100 kpc) radio jets in narrow-line seyfert 1 galaxies. *Astrophys. J.* 995, 125. doi:10.3847/1538-4357/ae19e7.
- Urry, C.M., Padovani, P., 1995. Unified schemes for radio-loud active galactic nuclei. *Publ. Astron. Soc. Pac.* 107, 803.
- Vagnetti, F., Trevese, D., Nesci, R., 2003. Spectral slope variability of bl lacertae objects in the optical band. *Astrophys. J.* 590, 123. doi:10.1086/374889.
- Vaughan, S., Edelson, R., Warwick, R., Uttley, P., 2003. On characterizing the variability properties of x-ray light curves from active galaxies. *Mon. Not. R. Astron. Soc.* 345, 1271. doi:10.1046/j.1365-2966.2003.07042.x.
- Vietri, A., Järvelä, E., Berton, M., Ciroi, S., Congiu, E., Chen, S., Di Mille, F., 2022. Spectacular 240 kpc double-sided relativistic jets in a spiral-hosted narrow-line seyfert 1 galaxy. *Astron. Astrophys.* 662, A20. doi:10.1051/0004-6361/202243523.
- Villata, M., Raiteri, C.M., Kurtanidze, O., Nikolashvili, M., Ibrahimov, M., Papadakis, I., Tosti, G., Hroch, F., Takalo, L., Sillanpää, A., et al., 2004. The webt bl lacertae campaign 2001 and its extension-optical light curves and colour analysis 1994–2002. *Astron. Astrophys.* 421, 103–114. doi:10.1051/0004-6361:20035895.
- Vince, O., Raiteri, C., Villata, M., Gupta, A., Kovačević-Dojčinović, J., Lakićević, M., Popović, L., Kushwaha, P., Mirzaqulov, D., Ehgamberdiev, S., et al., 2025. Multiband optical variability on diverse timescales of the blazar ton 599 from 2011 to 2023. *Astron. Astrophys.* 703, A259. doi:10.1051/0004-6361/202555986.
- Vlasyuk, V.V., Sotnikova, Y.V., Volvach, A.E., Mufakharov, T.V., Kovalev, Y.A., Spiridonova, O.I., Khabibullina, M.L., Kovalev, Y.Y., Mikhailov, A.G., Stolyarov, V.A., et al., 2024. Multiwavelength variability of the blazar ao 0235+ 164. *Mon. Not. R. Astron. Soc.* 535, 2775–2799. doi:10.1093/mnras/stae2491.
- Wagner, S.J., Witzel, A., 1995. Intraday variability in quasars and bl lac objects. *Ann. Rev. Astron. Astrophys.* 33, 163–197. doi:10.1146/annurev.aa.33.090195.001115.
- Wall, J.V., Danziger, I.J., Pettini, M., Warwick, R.S., Wamsteker, W., 1986. Pks 2005–489: a very bright bl lac object in a nearby galaxy. *Mon. Not. R. Astron. Soc.* 219, 23P–29P.
- Wall, J.V., Shimmins, A.J., Bolton, J.G., 1975. The parkes 2700 mhz survey (ninth part): Supplementary catalogue for the declination zone-45o to-65o. *Aust. J. Phys., Astrophys. Suppl.*, Vol. 34, p. 55 (1975) 34, 55.
- Wang, Y.F., Jiang, Y.G., 2020. A comprehensive study on the variation phenomena of ao 0235+ 164. *Astrophys. J.* 902, 41. doi:10.3847/1538-4357/abb36c.
- Wani, K.A., Gaur, H., 2020. X-ray flux and spectral variability of blazar h 2356-309. *Galaxies* 8, 59. doi:10.3390/galaxies8030059.
- Welsh, B.Y., Wheatley, J.M., Neil, J.D., 2011. Galex observations of quasar variability in the ultraviolet. *Astron. Astrophys.* 527, A15. doi:10.1051/0004-6361/201015865.
- White, N.E., Giommi, P., Angelini, L., 1994. Wgacat. *IAU Circ.* 6100, 1.
- Wierzcholska, A., Ostrowski, M., Stawarz, Ł., Wagner, S., Hauser, M., 2015. Longterm optical monitoring of bright bl lacertae objects with atom: Spectral variability and multiwavelength correlations. *Astron. Astrophys.* 573, A69. doi:10.1051/0004-6361/201423967.

- Wierzcholska, A., Wagner, S.J., 2016. X-ray spectral studies of TeV γ -ray emitting blazars. *Mon. Not. R. Astron. Soc.* 458, 56–83. doi:10.1093/mnras/stw095, arXiv:1601.07493.
- Woo, J.H., Urry, C.M., van der Marel, R.P., Lira, P., Maza, J., 2005. Black hole masses and host galaxy evolution of radio-loud active galactic nuclei. *Astrophys. J.* 631, 762. doi:10.1086/432681.
- Wood, K.S., Meekins, J.F., Yentis, D.J., Smathers, H.W., McNutt, D.P., Bleach, R.D., Byram, E.T., Chupp, T.A., Friedman, H., Meidav, M., 1984. The heao a-1 x-ray source catalog. *Astrophys. J. Suppl. Ser.* (ISSN 0067-0049), vol. 56, Dec. 1984, p. 507-649. NASA-Navy-supported research. 56, 507–649.
- Wu, J., Zhou, X., Ma, J., Jiang, Z., 2011. Optical variability and colour behaviour of 3c 345. *Mon. Not. R. Astron. Soc.* 418, 1640–1648. doi:10.1111/j.1365-2966.2011.19565.x.
- Yuan, W., Zhou, H.Y., Komossa, S., Dong, X.B., Wang, T.G., Lu, H., Bai, J.M., 2008. A population of radio-loud narrow-line seyfert 1 galaxies with blazar-like properties? *Astrophys. J.* 685, 801. doi:10.1086/591046.
- Zamaninasab, M., Clausen-Brown, E., Savolainen, T., Tchekhovskoy, A., 2014. Dynamically important magnetic fields near accreting supermassive black holes. *Nature* 510, 126–128. doi:10.1038/nature13399.
- Zeng, W., Hu, W., Zhang, G.M., Wen, T., Yang, S.B., Geng, X.F., Wu, X.H., Zhou, X.Z., Dai, B.Z., 2019. Minute-scale rapid variability of mrk 501 by multi-band photometric monitoring from 2010 to 2017. *Publ. Astron. Soc. Pac.* 131, 074102. doi:10.1088/1538-3873/ab200f.
- Zhou, D., Zhang, Z., Gupta, A.C., Kushwaha, P., Wiita, P.J., Gu, M., Xu, H., 2024. X-ray flux and spectral variability of the blazar OJ 287 with Suzaku. *Mon. Not. R. Astron. Soc.* 532, 3285–3298. doi:10.1093/mnras/stae1722, arXiv:2408.02371.
- Zhou, H., Wang, T., Yuan, W., Shan, H., Komossa, S., Lu, H., Liu, Y., Xu, D., Bai, J., Jiang, D.R., 2007. A narrow-line seyfert 1-blazar composite nucleus in 2max j0324+ 3410. *Astrophys. J.* 658, L13. doi:10.1086/513604.

Appendix A. Brightness measurements of the individual sources analyzed

Table A.1: Brightness measurements of 1ES 0120+340

Date	Filter	MJD start	MJD end	Mag
04-12-2018	F154W	58453.177916	58453.184880	19.92 ± 0.14
		58453.245573	58453.260578	19.64 ± 0.08
		58453.313235	58453.333842	19.71 ± 0.07
		58453.380897	58453.402049	19.65 ± 0.07
		58453.448559	58453.469700	19.77 ± 0.07
		58453.516222	58453.537350	19.78 ± 0.07
		58453.583886	58453.604995	19.68 ± 0.07
		58453.651547	58453.672646	19.63 ± 0.07
		58453.719209	58453.740296	19.69 ± 0.07
		58453.786872	58453.807947	19.73 ± 0.07
		58453.857090	58453.875597	19.77 ± 0.08
		58454.002228	58454.010898	19.68 ± 0.11
		58454.192834	58454.202939	19.75 ± 0.11
		58454.260497	58454.277244	19.69 ± 0.08
		58454.328159	58454.349151	19.69 ± 0.07
		58454.395822	58454.416802	19.72 ± 0.07
		58454.463478	58454.484453	19.65 ± 0.07
		58454.598803	58454.619754	19.62 ± 0.07
		58454.666465	58454.687404	19.66 ± 0.07
		58454.734128	58454.755055	19.73 ± 0.07
		58454.801798	58454.822706	19.72 ± 0.07
		58454.873063	58454.890356	19.73 ± 0.08
		58454.945632	58454.958007	19.54 ± 0.09
		58455.140091	58455.144602	19.60 ± 0.15
		58455.207753	58455.219950	19.78 ± 0.10
		58455.275415	58455.293561	19.72 ± 0.08
		58455.343071	58455.363898	19.55 ± 0.07
		58455.410734	58455.431548	19.60 ± 0.07
		58455.478396	58455.499199	19.70 ± 0.07
		58455.546058	58455.566849	19.66 ± 0.07
		58455.613723	58455.634500	19.85 ± 0.08
		58455.681383	58455.702150	19.68 ± 0.07
		58455.749040	58455.769801	19.78 ± 0.07
		58455.816704	58455.837452	19.75 ± 0.07
		58455.889036	58455.905102	19.70 ± 0.08
		58455.961949	58455.972753	19.54 ± 0.09
		58456.034518	58456.040391	19.49 ± 0.12
		58456.155009	58456.162310	19.61 ± 0.12
		58456.222665	58456.236616	19.80 ± 0.09
		58456.290327	58456.309536	19.65 ± 0.07
		58456.357989	58456.378632	19.58 ± 0.07
		58456.425651	58456.446282	19.77 ± 0.07
58456.493313	58456.513932	19.78 ± 0.08		
58456.560976	58456.581583	19.75 ± 0.07		

Table A.2: Brightness measurements of 1ES 0229+200

Date	Filter	MJD start	MJD end	Mag	
22-09-2017	F154W	58017.831844	58017.844789	20.50 ± 0.14	
		58017.897540	58017.914527	20.57 ± 0.12	
		58017.972337	58017.984271	20.41 ± 0.13	
		58018.047132	58018.054009	20.47 ± 0.18	
		58018.100982	58018.123759	20.66 ± 0.21	
		58018.170720	58018.174450	20.45 ± 0.24	
	F172M	58018.176239	58018.180995	20.16 ± 0.43	
		58018.240464	58018.255429	20.27 ± 0.26	
		58018.310208	58018.312937	19.78 ± 0.46	
		58018.379953	58018.402155	20.53 ± 0.25	
		58018.449691	58018.472473	20.31 ± 0.22	
		58018.519435	58018.542205	20.40 ± 0.23	
	N219M	58018.658923	58018.674273	19.91 ± 0.21	
		58017.831844	58017.844840	20.34 ± 0.24	
		58017.897490	58017.914578	20.30 ± 0.20	
		58017.972286	58017.984322	20.02 ± 0.20	
		58018.047082	58018.054060	20.32 ± 0.32	
		58018.100932	58018.105887	20.70 ± 0.47	
	N245M	58018.170670	58018.181046	20.20 ± 0.24	
		58018.240414	58018.246042	20.06 ± 0.30	
		58018.310158	58018.328846	19.98 ± 0.13	
		58018.379902	58018.402206	19.89 ± 0.06	
		58018.449640	58018.467429	19.95 ± 0.06	
		58018.469098	58018.472525	19.69 ± 0.15	
N263M	58018.519384	58018.542257	19.68 ± 0.06		
	58018.658872	58018.674346	19.77 ± 0.08		
	09-08-2021	F154W	59434.458958	59434.472963	20.16 ± 0.11
			59434.526603	59434.540631	20.66 ± 0.14
			59434.594241	59434.608293	20.48 ± 0.13
			59434.661886	59434.675956	20.29 ± 0.12
59434.729525			59434.743612	20.34 ± 0.12	
59434.797164			59434.811274	20.29 ± 0.12	
59434.864808			59434.878931	20.37 ± 0.12	
59434.932466			59434.946589	20.23 ± 0.11	
59435.005011			59435.014249	20.30 ± 0.15	
F169M		59435.077580	59435.080980	20.27 ± 0.24	
		59435.270657	59435.280022	20.26 ± 0.14	
		59435.338296	59435.351553	20.17 ± 0.11	
		59435.405940	59435.420211	20.23 ± 0.11	
		59435.473585	59435.481634	20.54 ± 0.18	
		59435.483371	59435.487862	20.20 ± 0.24	
		59435.541223	59435.555524	20.10 ± 0.13	
		59435.608868	59435.623186	20.34 ± 0.14	
		59435.676507	59435.690849	20.13 ± 0.13	
59435.744145	59435.758511	20.20 ± 0.13			
59435.811790	59435.826173	20.13 ± 0.13			

Date	Filter	MJD start	MJD end	Mag
		59435.879428	59435.893830	20.43 ± 0.15
		59435.948414	59435.961480	20.08 ± 0.13
		59436.020983	59436.029142	19.98 ± 0.16
		59436.420561	59436.435105	20.13 ± 0.13
		59436.555851	59436.570429	20.26 ± 0.14
		59436.623489	59436.638091	20.02 ± 0.12
		59436.691133	59436.701052	20.27 ± 0.17
		59436.758772	59436.773205	20.32 ± 0.14

Table A.3: Brightness measurements of AO 0235+164

Date	Filter	MJD start	MJD end	Mag
04-09-2016	F148W	57634.342759	57634.350027	23.10 ± 0.75
		57634.413129	57634.421919	22.93 ± 0.60
		57634.478083	57634.493996	23.36 ± 0.62
		57634.545752	57634.561670	23.49 ± 0.68
		57634.613414	57634.629344	22.77 ± 0.40
		57634.681076	57634.697012	22.91 ± 0.44
		57634.816407	57634.832354	22.43 ± 0.31
		57634.884982	57634.900029	22.42 ± 0.32
		57634.957551	57634.967697	22.79 ± 0.51
		57635.030120	57635.035362	21.99 ± 0.41
		57635.290055	57635.294142	22.54 ± 0.66
		57635.357723	57635.365671	22.21 ± 0.38
		57635.425979	57635.438240	22.60 ± 0.40
		57635.493048	57635.509061	23.00 ± 0.47
		57635.560716	57635.576735	22.71 ± 0.38
		57635.628378	57635.644409	22.34 ± 0.30
		57635.696041	57635.712077	23.64 ± 0.76
		57635.763703	57635.779751	22.78 ± 0.40
		57635.831371	57635.847420	22.78 ± 0.40
	N219M	57634.275042	57634.278564	20.73 ± 0.56
		57634.342710	57634.350096	21.27 ± 0.55
		57634.410373	57634.421968	21.04 ± 0.38
		57634.478035	57634.494045	21.02 ± 0.32
		57634.545703	57634.561719	20.98 ± 0.31
		57634.613365	57634.629394	20.93 ± 0.30
		57634.681027	57634.697062	20.58 ± 0.24
		57634.748690	57634.764736	20.89 ± 0.29
		57634.816358	57634.832404	20.62 ± 0.25
		57634.884933	57634.900078	20.74 ± 0.27
		57634.957502	57634.967747	20.81 ± 0.35
		57635.030071	57635.035412	21.19 ± 0.62
		57635.363170	57635.360296	20.69 ± 0.45
		57635.425337	57635.438289	20.94 ± 0.34
		57635.492999	57635.509110	20.94 ± 0.30
		57635.560667	57635.576784	21.05 ± 0.32
		57635.628329	57635.644459	20.85 ± 0.29
		57635.695992	57635.712127	21.14 ± 0.35
		57635.763654	57635.779801	20.59 ± 0.24
		57635.831322	57635.847469	20.95 ± 0.30

Table A.4: Brightness measurements of 1H 0323+342

Date	Filter	MJD start	MJD end	Mag
06-09-2020	F148W	59098.402173	59098.414745	17.93 ± 0.04
		59098.469829	59098.487177	17.98 ± 0.03
		59098.537480	59098.554834	17.95 ± 0.03
		59098.605136	59098.622490	17.99 ± 0.03
		59098.672797	59098.690146	17.98 ± 0.03
		59098.740443	59098.757547	17.95 ± 0.03
30-09-2020	F148W	59122.499163	59122.505618	17.84 ± 0.05
		59122.552051	59122.573280	17.87 ± 0.03
		59122.619695	59122.640937	17.86 ± 0.03
		59122.687334	59122.708593	17.87 ± 0.03
		59122.754973	59122.765409	17.92 ± 0.04
04-02-2022	F148W	59613.668914	59613.683080	17.86 ± 0.03
		59613.736565	59613.750724	17.85 ± 0.03
		59613.804235	59613.818363	17.81 ± 0.03
		59613.875145	59613.885996	17.81 ± 0.04
		59613.947714	59613.953635	17.90 ± 0.05
		59614.142462	59614.150161	17.85 ± 0.04
		59614.210113	59614.222731	17.82 ± 0.03
		59614.277764	59614.291816	17.80 ± 0.03
		59614.346997	59614.359449	17.83 ± 0.03
		59614.413064	59614.422499	17.76 ± 0.04

Table A.5: Brightness measurements of 1ES 0347–121

Date	Filter	MJD start	MJD end	Mag
21-08-2020	F148W	59082.304138	59082.312662	18.83 ± 0.06
		59082.371788	59082.383845	19.00 ± 0.06
		59082.439433	59082.450955	18.80 ± 0.06
		59082.507077	59082.519524	18.82 ± 0.05

Table A.6: Brightness measurements of PKS 0352–686

Date	Filter	MJD start	MJD end	Mag	
02-11-2018	F148W	58423.476028	58423.494365	19.66 ± 0.07	
		58423.540074	58423.562033	19.76 ± 0.06	
		58423.607732	58423.629696	19.69 ± 0.06	
		58423.675394	58423.697357	19.73 ± 0.06	
		58423.743056	58423.765020	19.65 ± 0.06	
		58423.811259	58423.832683	19.67 ± 0.06	
		58423.883828	58423.896043	19.57 ± 0.08	
		F154W	58423.956397	58423.967995	19.63 ± 0.09
			58424.028966	58424.035657	19.56 ± 0.12
			58424.081368	58424.103308	19.66 ± 0.13
			58424.149030	58424.157450	19.77 ± 0.12
			58424.216693	58424.228627	19.55 ± 0.09
		F148W	58424.284354	58424.299809	19.54 ± 0.08
			58424.352023	58424.370645	19.54 ± 0.07
	58424.419685		58424.441619	19.53 ± 0.07	
	58424.487347		58424.509282	19.64 ± 0.07	
	58424.555015		58424.569960	19.49 ± 0.08	

Table A.7: Brightness measurements of PKS 0447–439

Date	Filter	MJD start	MJD end	Mag
15-12-2017	F154W	58102.012648	58102.021247	16.31 ± 0.02
		58102.085217	58102.088921	16.30 ± 0.03
		58102.134934	58102.140782	16.32 ± 0.03
		58102.202597	58102.215087	16.30 ± 0.02
		58102.270259	58102.287656	16.29 ± 0.02
		58102.337922	58102.359535	16.31 ± 0.02
		58102.405584	58102.427239	16.28 ± 0.02
		58102.473252	58102.494907	16.29 ± 0.02
		58102.540915	58102.544877	16.21 ± 0.03
		F169M	58102.546607	58102.562569
	N245M	58102.012599	58102.021296	15.77 ± 0.01
		58102.085168	58102.088970	15.73 ± 0.02
		58102.134886	58102.140831	15.78 ± 0.01
		58102.202548	58102.215137	15.76 ± 0.01
		58102.270210	58102.287706	15.75 ± 0.01
		58102.337873	58102.359584	15.75 ± 0.01
		58102.405535	58102.427288	15.76 ± 0.01
		58102.473203	58102.494957	15.77 ± 0.01
		58102.540866	58102.544927	15.75 ± 0.02
		N263M	58102.546558	58102.562619

Table A.8: Brightness measurements of 1H 0658+595

Date	Filter	MJD start	MJD end	Mag
19-11-2016	F154W	57711.076889	57711.099403	18.99 ± 0.09
		57711.146694	57711.155726	18.96 ± 0.08
		57711.216492	57711.229507	18.88 ± 0.06
		57711.286291	57711.302930	18.92 ± 0.05
		57711.356095	57711.376347	18.98 ± 0.05
	F172M	57711.440560	57711.446928	18.77 ± 0.18
		57711.498570	57711.518192	18.43 ± 0.09
		57711.565498	57711.587991	18.62 ± 0.09
		57711.635315	57711.657789	18.50 ± 0.09
	N245M	57711.437081	57711.448446	18.50 ± 0.04
		57711.500361	57711.518244	18.51 ± 0.03
		57711.565446	57711.571027	18.45 ± 0.05
	N263M	57711.577500	57711.588043	18.41 ± 0.05
	N279N	57711.076839	57711.081639	18.39 ± 0.15
		57711.146643	57711.155777	18.41 ± 0.11
		57711.217441	57711.229558	18.43 ± 0.09
		57711.286240	57711.302981	18.29 ± 0.08
		57711.356045	57711.376398	18.39 ± 0.07
		57711.425843	57711.432454	18.35 ± 0.13

Table A.9: Brightness measurements of S5 0836+71

Date	Filter	MJD start	MJD end	Mag
04-05-2017	F154W	57875.583540	57875.605205	21.59 ± 0.19
		57875.651212	57875.672878	21.32 ± 0.16
		57875.718886	57875.740547	21.71 ± 0.20
		57875.786554	57875.808215	21.71 ± 0.20
		57875.857092	57875.875883	21.75 ± 0.22
		57875.929661	57875.943545	21.57 ± 0.23
		57876.002230	57876.011201	21.86 ± 0.35
		57876.074799	57876.078882	21.23 ± 0.35
		57876.327924	57876.349548	21.52 ± 0.18
		57876.395592	57876.417211	21.56 ± 0.19
		57876.463266	57876.484879	21.54 ± 0.18
		57876.530940	57876.552547	21.92 ± 0.23
		57876.598608	57876.620215	21.54 ± 0.18
		57876.666282	57876.687883	22.36 ± 0.31
		57876.733956	57876.755551	21.61 ± 0.19
		57876.801626	57876.823219	21.75 ± 0.21
		57876.873412	57876.890888	22.08 ± 0.29
		57876.945981	57876.958550	21.36 ± 0.22
		57877.019775	57877.026212	21.17 ± 0.27
		57877.139983	57877.143210	21.39 ± 0.44
		57877.207651	57877.219602	21.67 ± 0.27
		57877.275325	57877.293566	21.56 ± 0.20
		57877.342999	57877.364553	21.98 ± 0.24
		57877.410673	57877.432221	21.56 ± 0.19
		57877.478341	57877.499889	21.49 ± 0.18
		57877.546015	57877.567557	21.47 ± 0.18
		57877.613689	57877.635231	21.54 ± 0.18
		57877.681364	57877.702900	21.54 ± 0.18
		57877.749032	57877.770562	21.89 ± 0.23
		57877.816814	57877.838230	21.94 ± 0.24
		57877.889383	57877.905901	21.66 ± 0.23
		57877.961952	57877.973566	21.59 ± 0.26
		57878.034521	57878.041228	21.52 ± 0.33
		57878.155064	57878.161616	21.78 ± 0.39
		57878.222738	57878.236618	21.53 ± 0.23
		57878.290412	57878.309880	21.36 ± 0.17
		57878.358087	57878.379569	21.66 ± 0.21
		57878.425755	57878.447231	21.33 ± 0.16

Table A.10: Brightness measurements of OJ 287

Date	Filter	MJD start	MJD end	Mag
25-10-2020	F154W	59142.523770	59142.531976	17.19 ± 0.04
		59142.597723	59142.599689	17.24 ± 0.07
		59142.659065	59142.666768	17.24 ± 0.04
		59142.934485	59142.937971	17.11 ± 0.05
		59143.001761	59143.005620	17.23 ± 0.05
		59143.069241	59143.073284	17.24 ± 0.05
		59143.403196	59143.407451	17.27 ± 0.05
		59143.470846	59143.479222	17.36 ± 0.04
		59143.538496	59143.546884	17.34 ± 0.04
		59143.606141	59143.614546	17.31 ± 0.04
		59143.673792	59143.682197	17.30 ± 0.04
		59143.741442	59143.749859	17.36 ± 0.04
		59143.809094	59143.817521	17.42 ± 0.04
		59143.876737	59143.885172	17.36 ± 0.04
		59143.944381	59143.952834	17.35 ± 0.04
		59144.016166	59144.020484	17.28 ± 0.05
		59144.085220	59144.088147	17.32 ± 0.06
		59144.421032	59144.423424	17.41 ± 0.07
		59144.485573	59144.489828	17.40 ± 0.05
		59144.553217	59144.561759	17.34 ± 0.04
		59144.620868	59144.629421	17.44 ± 0.04
		59144.688512	59144.696345	17.34 ± 0.04
		59144.963319	59144.967709	17.36 ± 0.05
		59145.028620	59145.035371	17.46 ± 0.04
		59145.567932	59145.576634	17.41 ± 0.04
		59145.635576	59145.644296	17.47 ± 0.04
		59145.703221	59145.711958	17.45 ± 0.04
		59145.770871	59145.779615	17.38 ± 0.04
		59145.838516	59145.847265	17.38 ± 0.04
		59145.907987	59145.914927	17.43 ± 0.04
		59145.973824	59145.982589	17.42 ± 0.04
		59146.044592	59146.049963	17.40 ± 0.05
		59146.514990	59146.523864	17.42 ± 0.04
		59146.582635	59146.591526	17.39 ± 0.04
		59146.650279	59146.659176	17.39 ± 0.04
		59146.717929	59146.726839	17.37 ± 0.04
		59146.785574	59146.794501	17.39 ± 0.04
		59146.853218	59146.862163	17.41 ± 0.04
		59146.920869	59146.929808	17.44 ± 0.04
		59146.988515	59146.995301	17.44 ± 0.04
		59147.060562	59147.065138	17.36 ± 0.05
		59147.394392	59147.398772	17.47 ± 0.05
		59147.462042	59147.471100	17.48 ± 0.04
		59147.529685	59147.538762	17.40 ± 0.04
		59147.597331	59147.606424	17.35 ± 0.04
		59147.664976	59147.674075	17.46 ± 0.04
		59147.732627	59147.741737	17.45 ± 0.04
59147.800271	59147.809400	17.40 ± 0.04		
59147.867915	59147.877062	17.43 ± 0.04		

Date	Filter	MJD start	MJD end	Mag
		59147.935560	59147.944724	17.41 ± 0.04
		59148.003964	59148.012386	17.43 ± 0.04
		59148.076533	59148.080036	17.38 ± 0.06
		59148.409083	59148.415788	17.35 ± 0.04
		59148.476727	59148.485992	17.41 ± 0.04
		59148.544378	59148.552900	17.34 ± 0.04
		59148.618952	59148.621317	17.40 ± 0.07
		59148.679667	59148.688979	17.36 ± 0.04
		59148.747311	59148.756641	17.35 ± 0.04
		59148.814956	59148.824304	17.40 ± 0.04
		59148.882600	59148.891966	17.40 ± 0.04
		59148.950245	59148.959618	17.36 ± 0.04
		59149.019935	59149.027278	17.37 ± 0.04
		59149.092510	59149.094941	17.40 ± 0.07
		59149.356123	59149.358495	17.43 ± 0.07
		59149.423768	59149.427977	17.36 ± 0.05
		59149.559057	59149.568577	17.38 ± 0.04
		59149.626701	59149.636238	17.38 ± 0.04
		59149.694346	59149.703889	17.37 ± 0.04
		59149.761990	59149.771552	17.43 ± 0.04
		59149.829635	59149.839213	17.37 ± 0.04
		59149.897279	59149.906876	17.41 ± 0.04
		59149.964931	59149.974538	17.45 ± 0.04
		59150.035912	59150.042201	17.37 ± 0.04
		59150.370797	59150.375161	17.47 ± 0.05
		59150.438447	59150.448156	17.38 ± 0.04
		59150.506092	59150.515819	17.45 ± 0.04
		59150.573736	59150.583481	17.33 ± 0.03
		59150.641381	59150.651143	17.45 ± 0.04
		59150.709025	59150.718805	17.48 ± 0.04
		59150.776669	59150.786468	17.47 ± 0.04
		59150.844314	59150.854130	17.39 ± 0.04
		59150.911958	59150.921792	17.44 ± 0.04
		59150.979598	59150.989454	17.49 ± 0.04
		59151.051883	59151.057117	17.47 ± 0.05
		59151.385470	59151.388587	17.47 ± 0.06
18-11-2021	F154W	59535.873750	59535.887589	17.48 ± 0.03
		59535.942853	59535.955240	17.51 ± 0.03
		59536.015422	59536.022890	17.49 ± 0.04
		59536.414912	59536.427590	17.51 ± 0.03
		59536.482562	59536.496444	17.51 ± 0.03
		59536.550207	59536.564106	17.49 ± 0.03
		59536.617851	59536.631756	17.49 ± 0.03
		59536.685496	59536.699407	17.52 ± 0.03
		59536.753148	59536.767057	17.51 ± 0.03
		59536.820785	59536.834708	17.48 ± 0.03
		59536.888437	59536.902358	17.43 ± 0.03

Date	Filter	MJD start	MJD end	Mag
20-11-2021	F154W	59537.767828	59537.781827	17.47 ± 0.03
		59537.835472	59537.849478	17.45 ± 0.03
		59537.903130	59537.911921	17.46 ± 0.04
		59538.377030	59538.386623	17.47 ± 0.04
		59538.444286	59538.458149	17.39 ± 0.03
		59538.513955	59538.525995	17.44 ± 0.03
		59538.579581	59538.593646	17.45 ± 0.03
		59538.647225	59538.661296	17.43 ± 0.03
		59538.714870	59538.728946	17.36 ± 0.03
		59538.782514	59538.796609	17.36 ± 0.03
18-04-2023	F154W	59538.850159	59538.863612	17.40 ± 0.03
		60051.280169	60051.296579	18.38 ± 0.04
		60051.347784	60051.364183	18.44 ± 0.04
		60051.415393	60051.431774	18.44 ± 0.04
		60051.483008	60051.499383	18.51 ± 0.05
		60051.550617	60051.566974	18.49 ± 0.05
		60051.618232	60051.634577	18.47 ± 0.05
		60051.685841	60051.702168	18.51 ± 0.05
		60051.753450	60051.769777	18.49 ± 0.05
		60051.821321	60051.837369	18.56 ± 0.05
		60051.893891	60051.903710	18.56 ± 0.06
		60052.294334	60052.310542	18.51 ± 0.05
		60052.361942	60052.378145	18.60 ± 0.05
		60052.429557	60052.445737	18.59 ± 0.05
		60052.497166	60052.513346	18.64 ± 0.05
		60052.564781	60052.580937	18.61 ± 0.05
		60052.632392	60052.648540	18.61 ± 0.05

Table A.11: Brightness measurements of Mrk 180

Date	Filter	MJD start	MJD end	Mag	
25-10-2018	F148W	58415.633992	58415.645633	17.50 ± 0.03	
		58415.701625	58415.713295	17.51 ± 0.03	
		58415.769251	58415.780958	17.62 ± 0.03	
		58415.836884	58415.848620	17.52 ± 0.03	
		58415.904517	58415.916281	17.54 ± 0.03	
		58415.973063	58415.983939	17.56 ± 0.03	
		58416.242704	58416.248080	17.50 ± 0.04	
		58416.310336	58416.319606	17.53 ± 0.03	
		58416.377975	58416.389912	17.47 ± 0.03	
		58416.445613	58416.457574	17.55 ± 0.03	
		58416.513252	58416.525237	17.56 ± 0.03	
		58416.580885	58416.584151	17.47 ± 0.05	
		F154W	58416.585873	58416.592893	17.49 ± 0.04
			58416.648517	58416.660555	17.40 ± 0.03
			58416.716150	58416.728218	17.43 ± 0.03
			58416.783783	58416.795880	17.39 ± 0.03
			58416.851421	58416.863542	17.45 ± 0.03

Table A.12: Brightness measurements of Ton 599

Date	Filter	MJD start	MJD end	Mag
24-04-2020	F148W	58962.537295	58962.557688	19.29 ± 0.05
		58962.672613	58962.694573	19.25 ± 0.05
		58962.740270	58962.762224	19.17 ± 0.05
		58962.807940	58962.829892	19.18 ± 0.05
		58962.879655	58962.886370	19.08 ± 0.08
	F169M	58962.888109	58962.897536	18.82 ± 0.09
		58962.952224	58962.965211	18.92 ± 0.08
		58963.024793	58963.032849	18.54 ± 0.08
		58963.097363	58963.100517	18.74 ± 0.14
		58963.146220	58963.150500	18.32 ± 0.10
		58963.213876	58963.221333	18.62 ± 0.09
		58963.281533	58963.292515	18.52 ± 0.07
		58963.349195	58963.364041	18.41 ± 0.06
		58963.416852	58963.435567	18.57 ± 0.06
		58963.486657	58963.506485	18.38 ± 0.05
	F172M	58963.552170	58963.557386	18.58 ± 0.10
		58963.559120	58963.574136	18.06 ± 0.09
		58963.619828	58963.641809	17.92 ± 0.07
		58963.687483	58963.709459	17.72 ± 0.07
		58963.755146	58963.777122	17.94 ± 0.07
		58963.823059	58963.844784	18.10 ± 0.08
		58963.895628	58963.905821	18.34 ± 0.13

Table A.13: Brightness measurements of 4C +21.35

Date	Filter	MJD start	MJD end	Mag
25-04-2018	F148W	58233.540491	58233.562165	16.32 ± 0.02
		58233.608182	58233.609904	16.40 ± 0.04
	F172M	58233.611642	58233.629838	15.49 ± 0.03
		58233.675828	58233.697501	15.49 ± 0.03
		58233.743496	58233.765164	15.49 ± 0.03
		58233.811172	58233.832820	15.49 ± 0.03
		58233.883480	58233.891753	15.48 ± 0.04

Table A.14: Brightness measurements of OQ 334

Date	Filter	MJD start	MJD end	Mag
12-01-2020	F148W	58859.704781	58859.715569	16.37 ± 0.02
		58859.772426	58859.783237	16.37 ± 0.02
		58859.840070	58859.850893	16.13 ± 0.02
		58859.907714	58859.918550	16.36 ± 0.02
		58859.975378	58859.979071	16.44 ± 0.03
	F154W	58859.980809	58859.986206	16.16 ± 0.03
		58860.047023	58860.052696	16.25 ± 0.03
		58860.119592	58860.121525	16.26 ± 0.05
		58860.245949	58860.249121	16.14 ± 0.03
		58860.313599	58860.320648	16.33 ± 0.03
		58860.381244	58860.392162	16.45 ± 0.02
	F169M	58860.448894	58860.459818	16.61 ± 0.02
		58860.519803	58860.527475	16.36 ± 0.03
		58860.584189	58860.595137	16.59 ± 0.03
		58860.651834	58860.662799	16.63 ± 0.03
		58860.719484	58860.730455	16.56 ± 0.03
	F172M	58860.787129	58860.793514	16.53 ± 0.04
		58860.795252	58860.798112	16.05 ± 0.08

Table A.15: Brightness measurements of Mrk 501

Date	Filter	MJD start	MJD end	Mag		
25-03-2022	F154W	59662.314522	59662.326899	15.88 ± 0.02		
		59662.381648	59662.397732	15.87 ± 0.02		
		59662.449286	59662.466911	15.90 ± 0.02		
		59662.516919	59662.534562	15.89 ± 0.02		
		59662.584552	59662.602212	15.89 ± 0.02		
		59662.652190	59662.669863	15.90 ± 0.02		
		59662.719824	59662.737513	15.91 ± 0.02		
		59662.787456	59662.805152	15.90 ± 0.02		
		59662.855108	59662.872802	15.89 ± 0.02		
		59662.925496	59662.940453	15.90 ± 0.02		
		59663.003531	59663.008102	15.91 ± 0.03		
		59663.260909	59663.270652	15.88 ± 0.02		
		59663.328547	59663.341828	15.85 ± 0.02		
		59663.396180	59663.413010	15.88 ± 0.02		
		59663.463818	59663.481644	15.88 ± 0.02		
		59663.531457	59663.549295	15.88 ± 0.02		
		59663.599089	59663.616946	15.87 ± 0.02		
		59663.666728	59663.684596	15.87 ± 0.02		
		59663.734361	59663.752247	15.85 ± 0.02		
		59663.801999	59663.819898	15.85 ± 0.02		
		59663.869645	59663.887547	15.87 ± 0.02		
		59663.941124	59663.955198	15.84 ± 0.02		
		59664.013837	59664.022848	15.86 ± 0.02		
		59664.086262	59664.090499	15.82 ± 0.03		
		59664.140181	59664.143215	15.84 ± 0.03		
		59664.207819	59664.214747	15.85 ± 0.02		
		59664.275452	59664.285925	15.84 ± 0.02		
		59664.343091	59664.356757	15.85 ± 0.02		
		59664.410730	59664.427940	15.85 ± 0.02		
		59664.478369	59664.496390	15.84 ± 0.02		
		23-10-2022	F148W	59870.516163	59870.521029	15.81 ± 0.02
				59870.583801	59870.588656	15.74 ± 0.02
59870.651434	59870.656293			15.75 ± 0.02		
59870.719067	59870.723933			15.78 ± 0.02		
59870.786718	59870.791560			15.79 ± 0.02		
59871.192513	59871.197362			15.78 ± 0.02		
59871.260146	59871.264989			15.77 ± 0.02		
59871.327784	59871.332627			15.78 ± 0.02		
59871.395417	59871.400254			15.79 ± 0.02		
59871.463055	59871.467892			15.77 ± 0.02		
59871.530694	59871.535531			15.75 ± 0.02		
59871.598327	59871.603157			15.74 ± 0.02		
59871.665959	59871.670796			15.77 ± 0.02		
59872.818525	59872.820569			15.80 ± 0.03		
59873.153931	59873.158726			15.80 ± 0.02		
59873.221563	59873.226365			15.79 ± 0.02		
59873.289202	59873.294003			15.81 ± 0.02		
59873.356835	59873.361630			15.84 ± 0.02		
59873.425311	59873.428993			15.79 ± 0.02		
59873.492106	59873.496895			15.79 ± 0.02		
59873.629489	59873.632178			15.80 ± 0.03		
59873.695010	59873.699805			15.83 ± 0.02		
59873.762648	59873.767309			15.84 ± 0.02		

Date	Filter	MJD start	MJD end	Mag
		59874.168450	59874.173239	15.85 ± 0.02
		59874.236088	59874.240866	15.81 ± 0.02
		59874.303721	59874.308505	15.84 ± 0.02
		59874.372252	59874.376131	15.87 ± 0.02
		59874.438992	59874.443770	15.80 ± 0.02
		59874.506625	59874.511415	15.83 ± 0.02
		59874.574264	59874.579041	15.85 ± 0.02
		59874.643028	59874.646680	15.85 ± 0.02
		59874.709535	59874.714307	15.81 ± 0.02
		59874.777961	59874.781945	15.92 ± 0.02
		59874.847368	59874.849584	15.84 ± 0.03
		59875.115331	59875.117525	15.84 ± 0.03
		59875.182970	59875.187741	15.84 ± 0.02
		59875.250602	59875.255367	15.81 ± 0.02
		59875.318531	59875.323006	15.83 ± 0.02
		59875.385873	59875.390639	15.83 ± 0.02
		59875.455382	59875.458015	15.85 ± 0.03
		59875.589978	59875.593543	15.84 ± 0.03
		59875.656410	59875.661170	15.82 ± 0.02
		59875.724048	59875.728808	15.83 ± 0.02
		59875.791683	59875.796447	15.84 ± 0.02
		59876.129850	59876.134604	15.78 ± 0.02
		59876.197483	59876.202237	15.84 ± 0.02
		59876.265122	59876.269863	15.81 ± 0.02
		59876.332754	59876.337502	15.79 ± 0.02
		59876.401086	59876.405129	15.85 ± 0.02
		59876.468025	59876.472768	15.82 ± 0.02
		59876.535658	59876.540406	15.83 ± 0.02
		59876.603297	59876.608033	15.83 ± 0.02
		59876.740602	59876.743298	15.87 ± 0.03
		59876.806196	59876.809498	15.83 ± 0.03

Table A.16: Brightness measurements of 1H 1720+117

Date	Filter	MJD start	MJD end	Mag
10-05-2018	F148W	58248.765601	58248.787174	18.50 ± 0.04
		58248.833828	58248.845706	18.51 ± 0.05

Table A.17: Brightness measurements of S3 1741+19

Date	Filter	MJD start	MJD end	Mag	
23-08-2019	F154W	58717.672011	58717.689513	19.36 ± 0.07	
		58717.739674	58717.757170	19.55 ± 0.07	
		58717.807337	58717.824820	19.54 ± 0.07	
		58717.879314	58717.892471	19.50 ± 0.08	
		58717.951883	58717.960127	19.50 ± 0.10	
		58718.024452	58718.027765	19.28 ± 0.15	
		58718.213310	58718.223420	19.38 ± 0.09	
		58718.280972	58718.287319	19.37 ± 0.11	
		F172M	58718.289059	58718.295639	18.71 ± 0.17
			58718.348634	58718.366017	18.82 ± 0.11
	58718.416296		58718.433680	19.03 ± 0.12	
	58718.483959		58718.501330	19.05 ± 0.12	
	58718.551627		58718.568980	18.84 ± 0.11	
	58718.619289		58718.636631	18.90 ± 0.12	
	58718.754614		58718.771932	19.06 ± 0.12	
	58718.822716		58718.830209	18.44 ± 0.14	

Table A.18: Brightness measurements of IES 1959+650

Date	Filter	MJD start	MJD end	Mag
05-10-2016	F154W	57666.211111	57666.223330	16.29 ± 0.02
		57666.280721	57666.296546	16.27 ± 0.02
		57666.350324	57666.358387	16.28 ± 0.02
	N263M	57666.211060	57666.223381	15.54 ± 0.01
		57666.280670	57666.296596	15.53 ± 0.01
		57666.350274	57666.358438	15.54 ± 0.02
04-11-2016	F154W	57695.927007	57695.933389	16.32 ± 0.03
		57696.189999	57696.194833	16.32 ± 0.03
		57696.258474	57696.270917	16.27 ± 0.02
		57696.325341	57696.339523	16.30 ± 0.02
		57696.393010	57696.407209	16.28 ± 0.02
		57696.460684	57696.474901	16.29 ± 0.02
		57696.528352	57696.542593	16.29 ± 0.02
		57696.596028	57696.610279	16.33 ± 0.02
		57696.663695	57696.677971	16.29 ± 0.02
		57696.731363	57696.745663	16.29 ± 0.02
		57696.799049	57696.813349	16.27 ± 0.02
		57696.870416	57696.881041	16.25 ± 0.02
		57696.943331	57696.948733	16.20 ± 0.03
		57697.205052	57697.213243	16.21 ± 0.02
		57697.272726	57697.287157	16.23 ± 0.02
	57697.340395	57697.352093	16.22 ± 0.02	
	57698.221519	57698.231158	16.20 ± 0.02	
	57698.355447	57698.370098	16.19 ± 0.02	
	N279N	57695.926935	57695.933439	15.59 ± 0.03
		57696.193846	57696.193832	15.44 ± 0.04
		57696.258569	57696.271082	15.46 ± 0.02
		57696.325293	57696.339573	15.44 ± 0.02
		57696.392961	57696.407259	15.49 ± 0.02
		57696.460635	57696.474951	15.50 ± 0.02
		57696.528303	57696.542643	15.50 ± 0.02
		57696.595977	57696.610329	15.48 ± 0.02
		57696.663646	57696.678021	15.45 ± 0.02
		57696.731314	57696.745713	15.43 ± 0.02
		57696.798998	57696.813399	15.42 ± 0.02
		57696.870344	57696.881091	15.46 ± 0.03
57696.943256		57696.948783	15.45 ± 0.03	
57697.205003		57697.213293	15.46 ± 0.03	
57697.272677		57697.287207	15.44 ± 0.02	
57697.340346	57697.350800	15.37 ± 0.03		
57698.225161	57698.231158	15.36 ± 0.03		
57698.355399	57698.370147	15.40 ± 0.02		
16-11-2016	F154W	57708.444207	57708.452211	15.39 ± 0.02
	N263M	57708.444207	57708.452262	15.49 ± 0.02
		57708.507347	57708.521883	15.50 ± 0.01
		57708.576998	57708.585130	15.49 ± 0.02

Date	Filter	MJD start	MJD end	Mag	
25-10-2017	F154W	58051.181646	58051.186616	15.99 ± 0.03	
		58051.249315	58051.263010	15.99 ± 0.02	
		58051.316977	58051.334720	15.99 ± 0.02	
		58051.384645	58051.402394	15.99 ± 0.02	
		58051.452314	58051.470080	15.96 ± 0.02	
		58051.519976	58051.537754	15.94 ± 0.02	
		58051.587650	58051.605441	15.94 ± 0.02	
		58051.655312	58051.673115	15.96 ± 0.02	
		58051.722974	58051.740795	15.94 ± 0.02	
		58051.790646	58051.808469	15.94 ± 0.02	
		58051.861607	58051.875679	15.94 ± 0.02	
		N279N	58051.181597	58051.186666	15.35 ± 0.03
			58051.249266	58051.263060	15.25 ± 0.02
			58051.316928	58051.334770	15.24 ± 0.02
			58051.384596	58051.402444	15.27 ± 0.02
	58051.452264		58051.470130	15.21 ± 0.02	
	58051.519927		58051.537804	15.23 ± 0.02	
	58051.587601		58051.605490	15.18 ± 0.02	
	58051.655263		58051.673164	15.22 ± 0.02	
	58051.722925		58051.740844	15.22 ± 0.02	
	58051.790577		58051.808519	15.19 ± 0.02	
	58051.861558		58051.875729	15.17 ± 0.02	

Table A.19: Brightness measurements of PKS 2005–489

Date	Filter	MJD start	MJD end	Mag
15-10-2019	F148W	58771.266239	58771.266236	16.38 ± 0.02
		58771.332523	58771.331952	16.40 ± 0.02
		58771.394770	58771.409334	16.39 ± 0.02
		58771.462426	58771.465491	16.40 ± 0.03
		58771.467225	58771.476988	16.27 ± 0.02
	F154W	58771.530088	58771.544651	16.26 ± 0.02
		58771.597767	58771.612301	16.27 ± 0.02
		58771.665407	58771.673344	16.26 ± 0.02
		58771.675082	58771.679952	16.18 ± 0.03
	F169M	58771.733069	58771.747602	16.25 ± 0.02
		58771.800739	58771.815253	16.21 ± 0.02
		58771.872715	58771.881982	16.20 ± 0.03

Table A.20: Brightness measurements of CTA 102

Date	Filter	MJD start	MJD end	Mag		
21-07-2017	F148W	57954.350649	57954.366961	18.67 ± 0.04		
		57954.423957	57954.442245	18.68 ± 0.04		
		57954.489820	57954.511835	18.76 ± 0.04		
		57954.559405	57954.581426	18.70 ± 0.04		
		57954.636480	57954.651030	18.69 ± 0.05		
		57954.698568	57954.720615	18.70 ± 0.04		
		57954.768153	57954.790206	18.70 ± 0.04		
		57954.837750	57954.859796	18.59 ± 0.04		
		57954.912267	57954.929400	18.66 ± 0.04		
		57954.986905	57954.998990	18.61 ± 0.05		
		57955.061542	57955.068201	18.56 ± 0.06		
		57955.255247	57955.260098	18.79 ± 0.08		
		57955.324832	57955.335828	18.65 ± 0.05		
		57955.394417	57955.414037	18.78 ± 0.04		
		57955.464002	57955.486152	18.72 ± 0.04		
		57955.533587	57955.555743	18.73 ± 0.04		
		57955.603165	57955.625333	18.82 ± 0.04		
		57955.672750	57955.694931	18.73 ± 0.04		
		57955.742641	57955.742626	18.75 ± 0.04		
		57955.816035	57955.834112	18.86 ± 0.04		
		57955.882561	57955.900967	18.82 ± 0.04		
		N219M	N219M	57954.350598	57954.367012	17.85 ± 0.06
				57954.440418	57954.440144	17.83 ± 0.05
				57954.489770	57954.511887	17.86 ± 0.05
				57954.566116	57954.566102	17.80 ± 0.05
				57954.628939	57954.651081	17.74 ± 0.05
				57954.698518	57954.720666	17.73 ± 0.05
				57954.768103	57954.790256	17.84 ± 0.05
				57954.837676	57954.859847	17.69 ± 0.05
				57954.912217	57954.929451	17.83 ± 0.06
				57954.986854	57954.999042	17.77 ± 0.06
				57955.061492	57955.068201	17.77 ± 0.09
				57955.255197	57955.260170	17.68 ± 0.10
				57955.324782	57955.335879	17.81 ± 0.07
				57955.410185	57955.409246	17.78 ± 0.05
57955.463951	57955.486203			17.77 ± 0.05		
57955.533536	57955.555793			17.83 ± 0.05		
57955.603115	57955.625385			17.77 ± 0.05		
57955.672700	57955.694981			17.88 ± 0.05		
57955.742285	57955.764573			17.82 ± 0.05		
57955.811870	57955.834164			17.82 ± 0.05		
57955.882510	57955.901018			17.99 ± 0.06		
07-08-2019	F148W			58702.177816	58702.181066	18.91 ± 0.11
				58702.245472	58702.252243	18.92 ± 0.07
				58702.313129	58702.324118	18.99 ± 0.06
				58702.380791	58702.383449	19.07 ± 0.13
	F154W	58702.385187	58702.395169	18.90 ± 0.07		
	F172M	58702.516110	58702.538098	18.08 ± 0.07		
			58702.583767	58702.603028	18.44 ± 0.09	

Table A.21: Brightness measurements of 3C 454.3

Date	Filter	MJD start	MJD end	Mag
20-10-2016	F154W	57680.625139	57680.646044	18.26 ± 0.04
		57680.694799	57680.715692	18.31 ± 0.04
		57680.764458	57680.785339	18.35 ± 0.04
		57680.835828	57680.854987	18.28 ± 0.04
		57680.910526	57680.924606	18.30 ± 0.04
		57680.985224	57680.994276	18.29 ± 0.06
	F172M	57681.059922	57681.063923	18.22 ± 0.08
		57681.182410	57681.185489	18.26 ± 0.09
		57681.252076	57681.258760	18.33 ± 0.07
		57681.325185	57681.332386	17.83 ± 0.11
		57681.391395	57681.406728	17.90 ± 0.08
		57681.530715	57681.551437	17.87 ± 0.07
		57681.600375	57681.621084	17.90 ± 0.07
		57681.670035	57681.690731	17.80 ± 0.07
		57681.739693	57681.752560	17.81 ± 0.08
		N219M	57680.625089	57680.646095
	57680.694748		57680.715743	17.28 ± 0.04
	57680.764408		57680.768181	17.25 ± 0.09
	57680.844035		57680.855038	17.23 ± 0.05
	57680.910451		57680.924681	17.27 ± 0.05
	57680.985149		57680.994326	17.19 ± 0.06
	57681.059847		57681.063974	17.21 ± 0.09
	57681.252026		57681.258811	17.38 ± 0.07
	N279N	57681.325135	57681.332437	16.96 ± 0.06
		57681.391345	57681.406752	17.06 ± 0.04
		57681.530664	57681.551488	16.98 ± 0.04
57681.600324		57681.621135	17.03 ± 0.04	
57681.669985		57681.690783	16.97 ± 0.04	
57681.739643		57681.752560	17.02 ± 0.05	
27-06-2023	F154W	60121.662641	60121.669951	18.59 ± 0.07
	F169M	60121.671689	60121.678751	18.35 ± 0.08
		60121.730233	60121.746354	18.34 ± 0.05
		60121.797824	60121.809738	18.42 ± 0.06
	F172M	60121.811476	60121.813945	17.77 ± 0.17
		60121.865415	60121.881536	17.93 ± 0.08
		60121.934869	60121.949139	17.97 ± 0.08
		60122.080006	60122.084327	17.98 ± 0.14
		60122.270950	60122.273073	17.67 ± 0.18
		60122.406133	60122.417869	17.83 ± 0.08
		60122.473724	60122.489916	18.03 ± 0.08
		60122.541309	60122.548271	18.10 ± 0.12

Table A.22: Brightness measurements of IES 2322-409

Date	Filter	MJD start	MJD end	Mag
03-07-2020	F148W	59033.450076	59033.465859	17.76 ± 0.03
		59033.517732	59033.529611	17.77 ± 0.03
		59033.585388	59033.601190	17.74 ± 0.03
		59033.654843	59033.664081	17.71 ± 0.04

Table A.23: Brightness measurements of IES 2344+514

Date	Filter	MJD start	MJD end	Mag	
22-10-2017	F172M	58048.015081	58048.021983	19.09 ± 0.19	
		58048.207274	58048.209186	18.89 ± 0.33	
		58048.272010	58048.285228	19.13 ± 0.14	
	N245M	58047.952626	58047.955603	18.86 ± 0.09	
		58048.015032	58048.017860	18.95 ± 0.10	
		58048.207274	58048.209236	19.01 ± 0.12	
		58048.271963	58048.285277	18.91 ± 0.05	
		58048.271963	58048.285277	18.91 ± 0.05	
29-07-2021	F148W	59423.293892	59423.301899	19.28 ± 0.08	
		59423.357886	59423.377295	19.35 ± 0.06	
		59423.425530	59423.444951	19.36 ± 0.06	
		59423.493169	59423.512608	19.36 ± 0.06	
		59423.560808	59423.580258	19.32 ± 0.06	
		59423.628452	59423.647914	19.32 ± 0.06	
		59423.696091	59423.715571	19.36 ± 0.06	
		59423.763730	59423.775796	19.39 ± 0.07	
	F154W	59423.777535	59423.783215	19.25 ± 0.11	
		59423.831381	59423.850877	19.13 ± 0.06	
		59423.902232	59423.918534	19.22 ± 0.07	
		59423.974801	59423.986185	19.14 ± 0.08	
		59424.047719	59424.053719	19.20 ± 0.11	
		59424.304850	59424.319951	19.27 ± 0.07	
		59424.372495	59424.392110	19.21 ± 0.06	
		59424.440133	59424.459761	19.31 ± 0.06	
		59424.507772	59424.527418	19.21 ± 0.06	
		59424.575411	59424.582497	19.13 ± 0.10	
		F169M	59424.584238	59424.595068	18.92 ± 0.08
			59424.717534	59424.730381	19.15 ± 0.09
59424.778326	59424.791753		18.98 ± 0.08		
59424.845966	59424.865694		19.12 ± 0.07		
06-08-2021	F148W	59431.677512	59431.698943	19.42 ± 0.06	
		59431.745175	59431.766605	19.34 ± 0.05	
		59431.812850	59431.834268	19.36 ± 0.05	
		59431.884868	59431.901918	19.32 ± 0.06	
		59431.957438	59431.969580	19.39 ± 0.07	
		59432.030006	59432.037243	19.48 ± 0.10	
		59432.102232	59432.104905	19.21 ± 0.14	
		59432.152443	59432.157455	19.27 ± 0.10	
	F154W	59432.218793	59432.227750	19.25 ± 0.08	
		59432.294353	59432.305025	19.54 ± 0.08	
		59432.354112	59432.358599	19.30 ± 0.11	
		59432.360333	59432.375531	19.16 ± 0.07	
		59432.421774	59432.438368	19.25 ± 0.07	
		59432.557093	59432.578518	19.21 ± 0.06	
		59432.624756	59432.646175	19.24 ± 0.06	
		59432.692412	59432.713837	19.19 ± 0.06	
		F169M	59432.909076	59432.916806	19.29 ± 0.12
			59432.973066	59432.984457	19.27 ± 0.10
			59433.045635	59433.052119	19.41 ± 0.14
			59433.045635	59433.052119	19.41 ± 0.14

Table A.24: Brightness measurements of H 2356–309

Date	Filter	MJD start	MJD end	Mag		
17-10-2018	F154W	58407.368693	58407.390752	18.31 ± 0.04		
		58407.504017	58407.526088	18.23 ± 0.04		
		58407.571680	58407.593751	18.28 ± 0.04		
		58407.639342	58407.661413	18.22 ± 0.04		
		58407.707005	58407.729075	18.30 ± 0.04		
		58407.774667	58407.796731	18.23 ± 0.04		
		58407.844589	58407.864406	18.31 ± 0.04		
		58407.917158	58407.932069	18.23 ± 0.04		
		58407.989727	58407.998759	18.28 ± 0.06		
		58408.062296	58408.067393	18.22 ± 0.07		
		58408.248310	58408.263082	18.30 ± 0.04		
		58408.721952	58408.744029	18.29 ± 0.04		
		18-10-2023	F154W	60234.470743	60234.491343	18.80 ± 0.05
				60234.536763	60234.558922	18.79 ± 0.05
60234.604342	60234.626502			18.68 ± 0.04		
60234.671928	60234.694082			18.80 ± 0.05		
60234.739507	60234.761667			18.72 ± 0.04		
60234.807089	60234.820934			18.70 ± 0.05		
60234.891063	60234.896826			18.78 ± 0.09		
60234.952226	60234.964411			18.80 ± 0.06		
60235.024452	60235.031991			18.75 ± 0.08		
60235.077416	60235.099570			18.69 ± 0.08		
60235.415332	60235.437492			18.82 ± 0.05		
60235.482911	60235.505071			18.84 ± 0.05		
60235.550497	60235.572650			18.71 ± 0.04		
60235.618098	60235.640230			18.81 ± 0.05		
60235.685661	60235.707815			18.76 ± 0.04		
60235.753241	60235.775395			18.78 ± 0.05		
60235.822025	60235.833435	18.69 ± 0.06				